Special Section: Vadose Zone Modeling
Vadose Zone Journal

MODFLOW SURFACT: A State-of-the-Art Use of Vadose Zone Flow and Transport Equations and Numerical Techniques for Environmental Evaluations

Sorab Panday* and Peter S. Huyakorn

MODFLOW SURFACT is a state-of-the-art simulator that utilizes vadose zone flow and transport equations to provide practical solutions to the analysis of flow and contaminant transport at various levels of complexity and sophistication as needed for site evaluation and closure. The variably saturated flow equation can be solved with standard retention functions or with bimodal or multimodal relative permeability curves for unsaturated flow in porous and fractured systems. The equation can further be solved with pseudo-soil retention functions for confined–unconfined simulations and for use in wellbore hydraulics. Finally, the equation can be cast in terms of air phase flow to analyze subsurface air flow behavior. The variably saturated transport equation can be solved for an unsaturated medium or can be used for confined–unconfined situations. The passive phase of flow can be included in the equation to include both air and water phases in the transport situation. An immobile multicomponent nonaqueous phase liquid (NAPL) phase can further be included in the transport simulation with equilibrium partitioning providing mass transfer between phases, which adjusts NAPL saturations. Dual domain equations can be condensed into the transport equation to provide capabilities for analyzing transport in fractured media. General reaction capabilities provide analyses of complex environmental and geochemical interactions. Two examples are provided to demonstrate the value of a comprehensive simulation capability for site investigations.

Abbreviations: BTEX, benzene, toluene, ethylbenzene, and xylene; DCE, dichloroethylene; DNAPL, dense nonaqueous phase liquid; GSVE, gravity-segregated vertical equilibrium; NAPL, nonaqueous phase liquid; PCE, perchloroethylene; TCE, trichloroethylene; TVD, total variation diminishing; VC, vinyl chloride.

Investigations of pumping impacts and resource availability or analyses of contaminant migration or remediation at a site typically proceed from simple models that help understand or characterize the dominant site hydrogeologic conditions and general groundwater flow to more in-depth characterizations and evaluations of alternative and effective remedial designs that can include vadose zone flow; contaminant transport in the groundwater and the vadose zone; dominant wellbore effects on flow and transport for ambient conditions or remediation methodologies; multicomponent NAPL contaminant sources above and/or below the water table; fractured or dual-domain behavior; decaying or reacting conditions within all phases and all domains; and even investigations of air-phase remedial strategies such as air sparging or vacuum extraction. It is then highly advantageous to have these simulation capabilities in a single code that may be used to analyze all stages within the life cycle of a site investigation—from pilot studies to closure.

Benefits of a comprehensive simulation capability include (i) scalable solutions in terms of detail of conceptualization, ranging from simple evaluations to more complex and complete investigations; (ii) quick learning curve for additional capabilities as opposed to learning a suite of task-specific codes to be used at different stages of a site's life; (iii) consistent approximations throughout the analyses as opposed to possible differences in results from different codes owing to differences in gridding structures (e.g., rectangular, triangular, polygonal, tetrahedral, prismatic), spatial discretization approximations (e.g., finite-element, finite-difference, finite-volume); temporal discretization approximations (e.g., implicit, semi-implicit, explicit, higher order Runga-Kutta), and material property assignment schemes (node centered, element centered, etc.). Further, the tediousness and approximations involved in translating from one code to another are avoided: (iv) data preparation requirement progresses with complexity of analysis as opposed to generating all data, and maintaining updated files for all codes used at a site, as the complexity of the analyses increases; (v) consistent input–output data files for all analyses as opposed to having different codes with individual input–output structures and controls; and (vi) complete "mix-and-match" of all capabilities, as opposed to having to accept certain restrictions (e.g., on boundary conditions, discretization, single porosity, no volatization) of each code, within a set of task-specific codes.

The most comprehensive set of equations for evaluating multicomponent contaminant transport within multiple phases

HydroGeoLogic, Inc., 11107 Sunset Hills Rd., Suite 400, Reston, VA 20190; S. Panday, current address, Geomatrix Consultants, Inc., 620 Herndon Pkwy., Suite 200, Herndon, VA 20170. Received 21 Mar. 2007. *Corresponding author (spanday@geomatrix.com).

Vadose Zone J. 7:610–631
doi:10.2136/vzj2007.0052

in the subsurface are presented by the compositional approach (Corapcioglu and Panday, 1991; Panday et al., 1995). This equation set, however, becomes very challenging to solve and requires a very large computational burden even with the most robust numerical methods available, for even the simplest of situations. Robust compositional and multiphase models are described in Pruess (2004), Panday et al. (1995), Huyakorn et al. (1994a), and Forsyth (1994). The large computational burden of solving the compositional or multiphase set of equations arises primarily from having multiple equations at each node (one for each component of solution for a compositional model and one for each active phase of a multiphase solution). Panday and Corapcioglu (1989) presented an overview of how, under various simplifying assumptions, the compositional set of equation reduces to the multiphase flow equations, to the Richards equation for unsaturated flow, and ultimately to the saturated groundwater flow equation commonly used in groundwater analysis models such as MODFLOW. Thus, it is noted that appropriate simplifying assumptions can greatly reduce computational burden and still provide flexibility for a wide range of analysis. The high nonlinearity of the equation set also increases computational burden compared with the linear confined groundwater flow situation case. However, it should be noted that every other situation (except for the confined groundwater flow simulation case) is nonlinear; hence, robust and efficient nonlinear solution schemes are needed to provide quick and reliable computations for all but the simplest of situations.

The USGS modular finite-difference groundwater simulation code, MODFLOW (McDonald and Harbaugh, 1988; McDonald et al., 1991; Harbaugh and McDonald, 1996a,b), is probably the most used groundwater flow model worldwide, along with its transport simulation counterpart, MT3D (Zheng, 1990). Several modifications and additional capabilities have been incorporated into MODFLOW by USGS personnel and others since its development to make the code applicable for a wider range of groundwater flow situations (e.g., Prudic, 1989; Swain and Wexler, 1993; Jobson, 1989; Leake and Prudic, 1991; Hsieh and Freckleton, 1993; Cheng and Anderson, 1993; Hill, 1994; Leake and Lilly, 1997; Fenske et al., 1996; Goode and Appel, 1992). Associated models have also been developed from MODFLOW to expand the simulation capabilities. Examples include MF2K-FMP (MODFLOW 2000 with a farm management package), DAFLOW (MODFLOW 2000 with a diffusion-wave-approximation stream-flow routing package), MF2K-GWT (MODFLOW 2000 with a groundwater transport package), MF2K-GWM (MODFLOW 2000 with a groundwater management package), MF2K-LGR (MODFLOW 2000 with local grid refinement), MODBRANCH (a coupling of MODFLOW with the BRANCH model of flow through a network of rivers or streams), SEAWAT 2000 (MODFLOW 2000 with density dependent solute transport), and MF2K-VSF (MODFLOW 2000 with variably saturated flow). However, these models are not all integrated into one MODFLOW version (for instance, one cannot use the farm package along with variably saturated flow or with transport), nor is there an effort to do so because of possible incompatibilities. Furthermore, certain persistent limitations exist, whereby a MODFLOW simulation fails or gross assumptions are required to model specific site conditions. MODFLOW primarily encounters difficulties or requires conceptual restrictions in simulation of unconfined systems (which are nonlinear systems) and has a poor representation of wells. Additional difficulties are encountered when contaminant transport investigations are required after a MODFLOW simulation. The most popular transport code that links with MODFLOW is MT3D, which includes non-mass conservative method of characteristics schemes, is unable to handle transient flow conditions rigorously, encounters accuracy or stability problems, and has excessive computational requirements besides being limited to the saturated groundwater zone.

Thus, overcoming the difficulties and expanding the simulation capabilities of MODFLOW–MT3D solutions provided the basis for a comprehensive simulator that can be used for scoping studies as well as for detailed investigations. MODFLOW SURFACT achieves this by using the vadose zone flow and transport equations in unique ways to perform the wide range of analyses needed for understanding and managing water resources issues or contamination and remediation projects. The following sections detail the governing equations and related assumptions and limitations associated with the various uses of these equations. It is noteworthy that the wide variety of analysis capabilities is achieved by solving one flow equation per computational grid block decoupled from solution to one transport equation per contaminant species per grid block. Any greater detail in analysis or relaxation of the assumptions would require solving multiple coupled flow and/or transport equations for multiphase or compositional analyses requiring considerably more computational effort. Finally, it is noted that MODFLOW-SURFACT is an acronym indicating the additional modules developed for MODFLOW, which include *s*aturated and *u*nsaturated flow, *r*echarge, and *f*racture flow capabilities, and *a*nalysis of *c*ontaminant *t*ransport.

Governing Equations for Flow

This section discusses the governing equations for flow in various environmental settings and how they all relate to the vadose zone flow equation.

Three-Dimensional Variably Saturated Flow

The variably saturated groundwater flow equation (Huyakorn et al., 1986) provides a representation of flow in three-dimensional saturated–unsaturated systems and is expressed as

$$\frac{\partial}{\partial x}\left(K_{xx}k_{\mathrm{rw}}\frac{\partial h}{\partial x}\right)+\frac{\partial}{\partial y}\left(K_{yy}k_{\mathrm{rw}}\frac{\partial h}{\partial y}\right)+\frac{\partial}{\partial z}\left(K_{zz}k_{\mathrm{rw}}\frac{\partial h}{\partial z}\right)-W=\phi\frac{\partial S_{\mathrm{w}}}{\partial t}+S_{\mathrm{w}}S_{\mathrm{s}}\frac{\partial h}{\partial t} \quad [1]$$

where x, y, and z are Cartesian coordinates (L); K_{xx}, K_{yy}, and K_{zz} are the principal components of hydraulic conductivity along the x, y, and z axes, respectively (LT^{-1}); k_{rw} is the relative permeability, which is a function of water saturation; h is the hydraulic head (L); W is a volumetric flux per unit volume and represents sources and/or sinks of water (T^{-1}); ϕ is the porosity; S_{w} is the degree of saturation of water, which is a function of the pressure head; S_{s} is the specific storage of the porous material (L^{-1}); and t

is time (T). The variably saturated flow Eq. [1] rigorously models moisture movement in the unsaturated zone using soil moisture characteristic functions and relative permeability relations.

Two alternative functional expressions are commonly used to describe the relationship of relative permeability versus water saturation. These functions are given by Brooks and Corey (1966) as

$$k_{rw} = S_e^n \qquad [2a]$$

and by van Genuchten (1980) as

$$k_{rw} = S_e^{1/2}\left[1-\left(1-S_e^{1/\gamma}\right)^{\gamma}\right]^2 \qquad [2b]$$

where n and γ are empirical parameters and S_e is the effective water saturation, defined as $S_e = (S_w - S_{wr})/(1 - S_{wr})$, with S_{wr} being referred to as the residual water saturation.

The relationship of pressure head ($\Psi = h - z$, where z = vertically upward coordinate) versus water saturation is described by the following function (van Genuchten et al., 1977; Mualem, 1976):

$$S_e = \frac{S_w - S_{wr}}{1-S_{wr}} = \begin{cases} \dfrac{1}{\left[1+(\alpha h_c)^{\beta}\right]^{\gamma}} & \text{for } \Psi < 0 \\ 1 & \text{for } \Psi \geq 0 \end{cases} \qquad [3]$$

where α and β are empirical parameters, h_c is the capillary head defined as $(h_{ap} - \Psi)$, where h_{ap}, the pressure head in air, is taken as atmospheric (= 0), and S_{wr} is the residual water phase saturation. The parameters β and γ are related by $\gamma = 1 - 1/\beta$. The Brooks–Corey function for moisture retention is not implemented because it does not have smooth characteristics at full saturation. Note that a mixed use of the Brooks–Corey relative permeability function and the van Genuchten moisture retention function provides a practical solution that decouples the parameters of moisture retention from relative permeability. This provides greater flexibility in model calibration, although the modeler should be aware that the two curves are related.

Dual or multiple porosity unsaturated flow can be solved by a single equation per grid block by using the assumptions of Mohanty et al. (1997)—that superposition of the relative permeability curves for capillary-dominated and non-capillary-dominated flow can be performed based on the use of an average soil water tension representing the bulk soil (capillary and non-capillary domains)—thus alleviating the computational burden of solving multiple equations of a dual porosity system. A piecewise continuous hydraulic conductivity function (i.e., cut-and-join type as explained by Šimůnek et al., 2003) can be included in place of Eq. [2a] or [2b] to include a bimodal description of preferential flow pathways in the system. By this method, if the saturation in the system is less than a critical value S^*, the van Genuchten function of Eq. [2b] is used. However, when saturation is above S^*, an exponential conductivity curve is applied that increases conductivity rapidly near saturation, as follows:

$$k_r^* = \left(S^*\right)^{1/2}\left[1-\left(1-S^{*1/\gamma}\right)^{\gamma}\right]^2\left[1-\exp\left(S_e - S^*\right)\delta\right] \qquad [4]$$

where S^* is the critical or breakpoint saturation value at which flow changes from capillary dominated to non-capillary dominated and vice versa, k_r^* is the relative permeability when saturation is above S^*, and δ is a fitting parameter representing effective macroporosity or other structural features contributing to non-capillary dominated flow. An additional option for tabular input accommodates other functional forms. For instance, a tabular input of the function of Eq. [2b] can be used instead of the functional form to alleviate numerical difficulties that occur due to high nonlinearities when β is close to 1. This is because the piecewise linear interpolation between tabulated data points (even when spaced at 1% saturation increments) will alter the true function to avoid the extremely steep gradients that occur in relative permeability when the saturation is close to 1 for low values of β. Use of a tabular input may lead to discontinuous derivatives of the function, which could hinder Newton–Raphson calculations; however, experience has shown this effect to be minor compared with numerical difficulties encountered with low β values. Alternatively, it may be advantageous to use the Brooks–Corey relative permeability function of Eq. [2a], which is more smooth than its van Genuchten counterpart. Finally, it should be noted that the solution of the Richards equation for water flow assumes that air is a passive phase—that is, air flow is not solved for, but rather, air is allowed to instantaneously equilibrate with water flow via the constraint that $S_w + S_a = 1$. Thus, if there is resistance to flow of air in a system to allow it to quickly equilibrate to atmospheric conditions, it may be necessary to solve the multiphase equations with associated increased computational burden.

Confined–Unconfined Flow

The complexities of a variably saturated solution are often not justified or required. Furthermore, subsurface investigations begin with characterization and quantification of the unconfined and confined groundwater flow—as also required for water resource evaluations. To provide this simpler level of analysis, the vadose zone flow equation may be used with gravity-segregated vertical equilibrium (GSVE) concepts providing pseudo-soil functions (in lieu of Eq. [2] and [3]) that track the unconfined water table as detailed by Wu et al. (1994). Gravity-segregated vertical equilibrium assumes that the fluids (air and water for the unconfined flow situation) segregate vertically, with the denser fluid residing at the bottom. The retention curve is a step functions with residual saturation (zero) above the water table and a saturation of unity below (Huyakorn et al., 1994b). When integrated in the vertical direction over the grid block thickness, a pseudo-constitutive relation is developed that defines the functional relationship: $\overline{S}_w = S_w(\Psi)$ as a straight line, with $\overline{S}_w = 0$ when h = cell bottom or below and $\overline{S}_w = 1$ when h = cell top or above. A relative permeability of $k_{rw} = \overline{S}_w$ gives the equivalent relation to the Boussinesq transmissivity expression. Since integration is performed over only the grid-block thickness, GSVE requires instantaneous transfer of water vertically between grid blocks of a multilayered system above the water table. Therefore, the vertical direction k_{rw} is kept at unity to allow water to flow vertically under saturated conductivity conditions (which is more physical than "instantaneous"). By this method, the vadose zone flow equation may be used to solve for unconfined flow as in MODFLOW, but without the associated numerical difficulties of rewetting a dry domain. It should be further noted that the porosity in Eq. [1] represents the specific yield S_y, while analyzing confined–unconfined systems.

Well–Fracture Flow

Wells can have a significant impact on flow and contaminant transport behavior in the subsurface. Long well screens penetrating multiple aquifers extract water dynamically from the various layers depending on hydraulic conductivity and saturation conditions of the aquifers in their immediate vicinity. Long screen wells can have significant impact on flow behavior within or among aquifers even when they are not pumping. To include the impacts of active or abandoned wells on a simulation, a one-dimensional cylindrical well tube may be superposed or connected via well-loss equations to the porous matrix grid blocks as shown in Fig. 1. Within the well, the water is under GSVE conditions, and thus a one-dimensional form of the vadose zone flow equation along with GSVE curves provides a means for inclusion of well-dynamics effects into a simulation. The equation for flow through a well tube is expressed as

$$\frac{\partial}{\partial l}\left(K'_l k'_{\mathrm{rw}} \frac{\partial h'}{\partial l}\right) = \frac{\partial S'_{\mathrm{w}}}{\partial t} + S'_{\mathrm{w}} S'_{\mathrm{s}} \frac{\partial h'}{\partial t} \qquad [5]$$

where l is the distance along the well screen (L), K'_l is the hydraulic conductivity of the well (LT^{-1}), k'_{rw} is the relative permeability within the well, S'_{w} is the dimensionless saturated thickness of the well cell (ratio of saturated thickness to cell thickness), S'_{s} is the wellbore specific storage (L^{-1}), and h' is the hydraulic head in the well (L). Note that compressible storage of the well in Eq. [5] is typically zero. Gravity-segregated vertical equilibrium curves determine that the water level in the well cells is accurately represented. Note that k'_{rw} becomes zero when the well cell is dry and water can be transmitted vertically only through the porous medium system under these conditions. The saturated hydraulic conductivity of the well bore is estimated from laminar flow theory by applying the Hagen–Poiseuille equation (Sudicky et al., 1995):

$$K'_l = \frac{\rho g}{8\mu} r_{\mathrm{w}}^2 \qquad [6]$$

where ρ is the density of water (ML^{-3}), g is the gravitational acceleration (LT^{-2}), μ is the viscosity of water ($\mathrm{ML}^{-1}\,\mathrm{T}^{-1}$), and r_{w} is the radius of the well (L). Typically, well hydraulic conductivity values are orders of magnitude larger than interblock hydraulic conductivities of the porous matrix, making the results insensitive to well conductivity (whatever comes to the well from the aquifer can flow down the well bore) unless the well radius is very small, restricting flow in the wellbore.

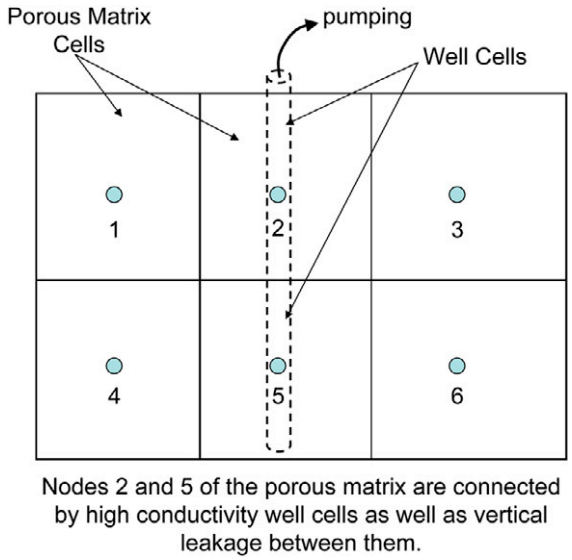

FIG. 1. Conceptualization of a fracture or well.

For an overpumped system, the total well withdrawal is further adjusted when the water level in the well reaches the screened bottom at any time step or iteration. At this stage, the hydraulic head at the bottom well node is fixed to screen bottom elevation, and the total withdrawal is computed to correspond to the feasible quantity that the well can supply under these conditions with a nonnegativity constraint. If the reverse situation occurs, whereby the withdrawal demand is less than what the well can supply at bottom-hole pressure conditions (e.g., if the pump is shut off for a particular period or recharge is increased), the boundary condition is again switched to the prescribed withdrawal condition and the computed hydraulic heads at the well nodes will bounce back to reflect these new conditions.

Air Phase Flow

Remedial technologies such as soil vapor extraction, air sparging, or in situ enhanced biodegradation require solving the air phase flow dynamics to appropriately assess their effectiveness. The vadose zone flow equation Eq. [1] can be readily modified to analyze air flow behavior. The flow of air in a variably saturated porous medium may be expressed as (Huyakorn et al., 1994a):

$$\frac{\partial}{\partial x_i}\left[\frac{k_{oij} k_{\mathrm{ra}} \rho_{\mathrm{a}}}{\mu_{\mathrm{a}}} \frac{\partial}{\partial x_j}\left(P_{\mathrm{a}} + \rho_{\mathrm{a}} g z\right)\right] - \rho_{\mathrm{a}} W_{\mathrm{a}} = \frac{\partial}{\partial t}\left(\phi \rho_{\mathrm{a}} S_{\mathrm{a}}\right) \qquad [7]$$

where x_i, x_j (i, j = 1, 2, 3) are Cartesian coordinates, k_{oij} is the intrinsic permeability tensor, k_{ra} is the relative permeability to air, μ_{a} is the dynamic viscosity of air, P_{a} is the pressure in the air phase, ρ_{a} is the density of air, W_{a} is the volumetric flux of air per unit volume of porous medium representing sources and/or sinks of air, and S_{a} (= 1 − S_{w}) is the air phase saturation.

For solution of Eq. [7] within the framework of the vadose zone water flow Eq. [1], it is convenient to express the equation in terms of hydraulic head. Equivalent definitions to pressure head and hydraulic head are therefore required for the air phase as

$$h_{\mathrm{ap}} = \frac{P_{\mathrm{a}}}{\rho_{\mathrm{w}} g} = \frac{\Phi_{\mathrm{a}}}{\rho_{\mathrm{w}} g} - \frac{\rho_{\mathrm{a}} g z}{\rho_{\mathrm{w}} g} = h_{\mathrm{a}\Phi} - \frac{\rho_{\mathrm{a}}}{\rho_{\mathrm{w}}} z \qquad [8]$$

where h_{ap} is the pressure head of the air phase, Φ_{a} is the potential in the air phase, ρ_{w} is the density of water, g is gravitational acceleration, and $h_{\mathrm{a}\Phi}$ is the potential head or total head in the air phase. Further, by definition, the hydraulic conductivity K_{ij} may be expressed as

$$K_{ij} = \frac{k_{oij} \rho_{\mathrm{w}} g}{\mu_{\mathrm{w}}} \qquad [9]$$

The first term on the left-hand side of Eq. [7] may therefore be manipulated using Eq. [8] and [9] and rewritten as

$$\frac{\partial}{\partial x_i}\left[\frac{k_{oij}k_{ra}\rho_a}{\mu_a}\frac{\partial}{\partial x_j}\left(P_a+\rho_a g z\right)\right]$$
$$=\frac{\partial}{\partial x_i}\left[\frac{k_{oij}k_{ra}\rho_a}{\mu_a}\rho_w g\frac{\partial}{\partial x_j}\left(h_{a\Phi}\right)\right] \quad [10]$$
$$=\frac{\partial}{\partial x_i}\left[K_{ij}\frac{\mu_w}{\mu_a}k_{ra}\rho_a\frac{\partial}{\partial x_j}\left(h_{a\Phi}\right)\right]$$

The last term in Eq. [7] may be manipulated for the air phase in an analogous manner, as was done by Bear (1979, p. 91) for the water phase, to give

$$\frac{\partial}{\partial t}\left(\phi\rho_a S_a\right)\approx\rho_a\phi\frac{\partial S_a}{\partial t}+\rho_a S_a S_{sa}\frac{\partial h_{a\Phi}}{\partial t} \quad [11]$$

where S_{sa} is a volumetric specific storage to air defined analogously as

$$S_{sa}=\rho_a g\left(\alpha_s+\phi\beta_a\right) \quad [12]$$

where α_s is the compressibility of the soil matrix and β_a is the compressibility of air. S_{sa} is not a tangible parameter for most aquifer systems, and further manipulation is required to pose the equation in terms of S_s, the specific storage of the porous material, defined as (Bear, 1979)

$$S_s=\rho_w g\left(\alpha_s+\phi\beta_w\right) \quad [13]$$

where β_w is the compressibility of water. Equations [12] and [13] yield

$$S_{sa}=\frac{\rho_a}{\rho_w}\left[S_s+\rho_w g\phi\left(\beta_a-\beta_w\right)\right] \quad [14]$$

Using Eq. [10], [11], and [14] in Eq. [7] gives the air phase flow equation in terms of hydraulic head and basic parameters as

$$\frac{\partial}{\partial x_i}\left[K_{ij}\frac{\mu_w}{\mu_a}k_{ra}\frac{\partial}{\partial x_j}\left(h_{a\Phi}\right)\right]-W_a$$
$$=\phi\frac{\partial S_a}{\partial t}+S_a\frac{\left[S_s+\rho_w g\phi\left(\beta_a-\beta_w\right)\right]}{\left(1+\rho_a\beta_a g Z\right)}\frac{\partial h_\Phi}{\partial t} \quad [15]$$

Note that the last term of Eq. [15] is the compressible storage term, which is significant in transient simulations that investigate subsurface air flow due to atmospheric pressure fluctuations. The denominator of this term is close to unity; however, the entire form has been retained for completeness.

The van Genuchten capillary pressure function of Eq. [6] provides the saturation distribution within the porous medium with the constraint that $S_w + S_a = 1$. Relative permeability to the air phase is expressed by the Brooks–Corey relationship as

$$k_{ra}=S_{ea}^2\left(1-S_e^{n-2}\right) \quad [16]$$

where S_{ea} is the effective air saturation defined analogously to the effective water saturation S_e, (see Eq. [6]) as

$$S_{ea}=\frac{S_a}{1-S_{wr}} \quad [17]$$

Note that the Brooks–Corey parameter n has to be greater than 2 for physically realistic k_r functions when air is the active phase. Relative permeability to the air phase is expressed by the van Genuchten relationship as

$$k_{ra}=S_{ea}^{1/2}\left(1-S_e^{1/\gamma}\right)^{2\gamma} \quad [18]$$

Equations [17] and [18] were obtained as three-phase extensions of network model expressions by Kaluarachchi and Parker (1989). Tabular input options provide further flexibility in allowing bimodal or multimodal inputs for fractured systems. When solving for the air phase flow equation only, an assumption has to be made regarding the water phase in the system, since water is treated as a passive phase. Two options provide treatment of the water phase when solving for air phase flow.

As a first option, water is assumed to be in hydrostatic equilibrium with a constant hydraulic head, equal to the initial elevation of the water table, ZWT (x,y), at any x, y location in the domain. The pressure head in the water phase, h_{wp} (= ψ used previously) at any elevation z within the domain is therefore given as

$$h_{wp}=\mathrm{ZWT}-z \quad [19]$$

where water pressure head, h_{wp} equals the ambient air pressure head (= 0) at the water table. The capillary head required in Eq. [3] ($h_c = h_{ap} - h_{wp}$) is therefore obtained using Eq. [19] and Eq. [8] as

$$h_c=h_{a\Phi}-\mathrm{ZWT}+\left(1-\frac{\rho_a}{\rho_w}\right)z \quad [20]$$

As a second option, the ambient hydraulic head of water may be obtained for Eq. [3] from a steady-state solution to the water flow equation over the same domain. Thus recharging–discharging systems may be accommodated during air phase flow calculations by providing correct air and water saturations under ambient air conditions. It should be noted that the passive water assumption implies that the flow equation for water is not solved and that water instantly equilibrates with air flow such that $S_w + S_a = 1$. Numerical experiments suggest that there is very little difference between results of solving the two-phase air–water flow equations and solving the air-phase flow equation with passive water assumption for typical air-sparging and vacuum extraction situations and for examining the effects of atmospheric pressure changes on subsurface water. Ultimately, the solution for saturation needs to lie at the same location on the equilibrium moisture-retention curve for the same capillary pressure situation when hysteresis is neglected. However, if there is high resistance to equilibration of water in the modeled situation, it may be necessary to solve the multiphase equations with associated increased computational burden.

The density of air at system pressure conditions is obtained from the ideal gas law as

$$\frac{\overline{P}_a}{\rho_a}=\frac{P_{atm}}{\rho_{std}} \quad [21]$$

where ρ_{std} is the standard air density at atmospheric pressure conditions, P_{atm}; $\overline{P}_a$ is the absolute pressure of air in the system; and it is assumed that the apparent molecular weight of air is the same for system conditions, as it is for standard conditions.

Rearranging Eq. [8] and expressing the air pressure under absolute pressure conditions gives

$$\overline{P}_a = \rho_w g h_{a\Phi} - \rho_a g z + P_{atm} \quad [22]$$

where the reference pressure P_{atm} occurs at the reference elevation $z = 0$ (i.e., at the datum). Density effects of air on the system potential are usually small, and one may prescribe P_{atm} for mean sea level conditions regardless of the datum elevation, without significant loss in accuracy. However, density effects of air are significant on the storage term.

Substituting Eq. [22] into Eq. [21] and rearranging gives the air phase density in terms of the vadose zone water flow equation variables as

$$\rho_a = \rho_{std} \frac{\left(\rho_w g h_{a\Phi} + P_{atm}\right)}{\left(\rho_{std} g z + P_{atm}\right)} \quad [23]$$

It should be noted that the air phase compressibility β_a in Eq. [15] may be obtained as the inverse of the absolute air pressure $\overline{P}_a$. However, use of a constant user-input value affects the solution very little. Summarizing the formulation for variably saturated air phase flow, Eq. [15] governs air flow behavior subject to capillary-saturation relations of Eq. [3] and relative permeability behavior of Eq. [16] or [18]. Capillary head is determined from Eq. [20] with a passive water phase assumption of instant hydrostatic equilibrium for water, or as $h_c = h_{ap} - h_{wp}$ with the ambient h_{wp} as input (possibly obtained from a water flow solution). Finally, air phase density is computed from Eq. [23].

In addition to the parameters required for soil moisture relations and relative permeability functions, air phase flow simulations also require input for ρ_w, μ_w, μ_a, β_w, β_a, P_{atm}, g, and ZWT (x,y) or hydraulic head in the water phase.

Governing Equations for Contaminant Transport

This section discusses the governing equations for transport under various environmental settings and how they can be solved under the umbrella of the vadose zone transport equation.

Three-Dimensional Variably Saturated Transport in Water

The partial differential equation governing three-dimensional transport of a contaminant species, k, in a variably saturated porous medium may be written in the primitive form as follows (Bear, 1979):

$$\begin{aligned}&\frac{\partial}{\partial x_i}\left(D_{ij}^k \frac{\partial c^k}{\partial x_j}\right) - \frac{\partial}{\partial x_i}\left(v_i c^k\right) = \frac{\partial}{\partial t}\left(\phi S_\alpha c^k\right) \frac{\partial}{\partial t}\left(\rho_B c_s^k\right)\\ &+\lambda_\alpha^k \phi S_\alpha c^k + \lambda_s^k \rho_B c_s^k - q c^{*k} + \Gamma^k\\ &- \sum_{j=1}^{NPAR} \xi_{kj} \lambda_\alpha^j \phi S_\alpha c^j - \sum_{j=1}^{NPAR} \xi_{kj} \lambda_s^j \rho_B c_s^j\\ &i \text{ or } j = 1,2,3\end{aligned} \quad [24]$$

where D_{ij} is the apparent hydrodynamic dispersion tensor; c^k is solute concentration of component k in the active phase; c_s^k is the concentration of component k adsorbed to the soil; v_i is the Darcy velocity; ϕ is the effective porosity; S_α is the saturation of the active fluid phase α; λ_α^k and λ_s^k are the first-order decay coefficients for component k in the active fluid phase α and soil, respectively, and may be computed from the half-life ($t_{1/2}$) of a radionuclide component from $\lambda = \ln 2/t_{1/2}$; q is the volumetric flow rate via sources (or sinks) per unit volume of the porous medium; c^{*k} is the solute concentration of the sources (or sinks); and Γ is the mass transfer rate of component k from the active phase to the inactive phase (which is zero for contaminant transport in the active phase only; i.e., it is displayed here for later generalization of the equation to include mass transfer). Component (j) is the parent component for daughter product k when transformation products occur, and the last two terms in Eq. [24] represent generation of component k as a result of decay of all parents j = 1 to NPAR (where NPAR is the number of immediate parents of k) in water and on soil, respectively. ξ_{kj} is the fraction of parent component j transforming into component k (which is unity for a straight chain decay where one unit of parent produces one unit of daughter), which can be determined from reaction stoichiometry and molecular weight. Equation [24] expresses the transport of a decaying contaminant in a sorbing porous medium because of advection and Fickian dispersion in the active phase. The sorbed and dissolved concentrations of component k are related by the nonlinear equilibrium Freundlich isotherm expressed as

$$c_s^k = \kappa^k \left(c^k\right)^{\left[\eta^k\right]} \quad [25]$$

where κ^k and η^k are the Freundlich coefficient and exponent respectively, for component k. Note that setting η^k to unity provides a linear isotherm for adsorption of component k.

The hydrodynamic dispersion tensorial components are computed using two-parameter constitutive relations for isotropic porous media (Scheidegger, 1961), the three-parameter relations for anisotropic media with dominantly horizontal flow (Burnett and Frind, 1987), or the four-parameter relations for stratified systems with three-dimensional flow (Guvanasen, personal communication, 1999). The longitudinal dispersivity of the two-component equation is typically an order of magnitude larger than the transverse dispersivity. For the three-component equations, the vertical transverse dispersivity is typically an order of magnitude less than the horizontal transverse dispersivity for areally extensive systems. For the four-component equations, the vertical and horizontal components of dispersion can be an order of magnitude apart for their respective longitudinal and transverse components. It should be noted that the four-component equations reduce to the three-component equations when the longitudinal vertical and longitudinal horizontal components of dispersivity are equal. It should also be noted that the three-component equations reduce to the two-component equations when the transverse vertical and transverse horizontal components of dispersivity are equal.

Transport Eq. [24] is valid for unsaturated zone transport in water when water is the active fluid phase solved by the flow equation. This equation further represents unsaturated zone transport in the air phase when air is the active fluid phase solved by the flow equation as discussed earlier in the section "Air Phase Flow."

Transport in Confined–Unconfined Groundwater

The storage term for contaminant concentration in the active phase (first term on the right-hand side of Eq. [24]) is expanded for the case of transport in a transient unsaturated flow field wherein the specific yield (S_y) values used in Eq. [1] for flow are

chosen to be different (smaller) than the porosity (ϕ) values of Eq. [24] for transport. For such cases, the storage of contaminant occurs within two regions of the pore space within any grid block. The first region includes the space occupied by the term S_y, and the second region includes the remaining pore space ($\phi - S_y$). For example, with the unconfined flow solution using GSVE functions, the specific yield measures only the drainable porosity, the remaining pore space being filled by water that is immobile. Thus, expanding the storage term gives

$$\frac{\partial}{\partial t}\left(\phi S_\alpha c^k\right)=\frac{\partial}{\partial t}\left[S_y S_\alpha c^k+\left(\phi-S_y\right)S_{\text{active}}c^k\right] \quad [26]$$

where S_{active} is the saturation of the active phase in the remaining pore space ($\phi - S_y$). This expansion is needed because the change of saturation of fluid is calculated as per space S_y, occurring due to net inflow minus outflow (which is used for the Darcy velocity in the transport equation). The remaining space is not involved in the flow equation, and it may optionally be assumed to be filled by the active phase ($S_{\text{active}} = 1$) or by the inactive phase ($S_{\text{active}} = 0$).

This is an important consideration when solving transport in a transient flow field with porosity and specific yield having different values. If it is not included (specifically in solutions that use the reduced form of the transport equation whereby a velocity is calculated as internodal flux divided by porosity), the flow field generated by injection or pumping within the smaller pore space S_y of the flow solution is used to provide the velocity distribution within the much larger pore space ϕ of the transport solution, which would have required proportionately more injection or extraction fluxes to generate. This is apparently the case with the MODFLOW–MT3D duo, and hence the specific yield and porosity values of the two codes need to be the same for meaningful solutions.

Transport in Both Air and Water Phases

Under conditions of unsaturated flow of air or water, it is possible to investigate mass transfer of contaminant from the active phase (defined as the phase that is active to flow) to the passive phase with associated storage, decay, generation, and diffusion occurring in the passive phase. Thus, for water being the active phase, a volatile contaminant would transfer mass into the air phase and diffuse in the air phase as well (advection in the air phase being neglected). Similarly, a contaminant in an active air phase may dissolve in the water phase and be transported by diffusion therein, neglecting water phase advection. The diffusive mass transport equation for contaminant k in the inactive phase may be expressed as

$$\frac{\partial}{\partial x_i}\left[\left(D_{ij}^k\right)_{\text{p}}\frac{\partial c_{\text{p}}^k}{\partial x_j}\right]= \frac{\partial}{\partial t}\left(\phi S_{\text{p}} c_{\text{p}}^k\right)+\lambda_{\text{p}}^k\phi S_{\text{p}}c_{\text{p}}^k-\sum_{j=1}^{\text{NPAR}}\xi_{kj}\lambda_{\text{p}}^j\phi S_{\text{p}}c_{\text{p}}^j-\Gamma^k \quad [27]$$

where the subscript p denotes the inactive (or passive) phase in the flow system solved by the flow modules, and Γ^k is the mass transfer term for contaminant k from the active phase to the inactive phase.

Equilibrium mass partitioning may be assumed between air and water phases (one of which is the active phase, the other being inactive with respect to the flow equation) to express the concentration of contaminant k in the air phase, c_a^k, as a function of its concentration in the water phase, as

$$c_{\text{a}}^k = K_{\text{aw}}^k c_{\text{w}}^k \quad [28]$$

Finally, summing Eq. [24] and [27] gives the governing equation for transport in both air and water phases as

$$\begin{aligned}&\frac{\partial}{\partial x_i}\left\{\left[D_{ij}^k+K_{\text{p}\alpha}^k\left(D_{ij}^k\right)_{\text{p}}\right]\frac{\partial c^k}{\partial x_j}\right\}-\frac{\partial}{\partial t}\left(v_i c^k\right)\\ &=\frac{\partial}{\partial t}\left[\phi\left(S_\alpha+K_{\text{p}\alpha}^k S_{\text{p}}\right)c^k\right]+\frac{\partial}{\partial t}\left(\rho_{\text{B}}c_{\text{s}}^k\right)\\ &+\left(\lambda_\alpha^k\phi S_\alpha+\lambda_{\text{p}}^k\phi S_{\text{p}}K_{\text{p}\alpha}^k\right)c^k+\lambda_{\text{s}}^k\rho_{\text{B}}c_{\text{s}}^k-qc^{*k}\\ &-\sum_{j=1}^{\text{NPAR}}\xi_{kj}\left(\lambda_\alpha^j\phi S_\alpha+\lambda_{\text{p}}^j\phi S_{\text{p}}K_{\text{p}\alpha}^j\right)c^j\\ &-\sum_{j=1}^{\text{NPAR}}\xi_{kj}\lambda_{\text{s}}^j\rho_{\text{B}}c_{\text{s}}^j\\ &i \text{ or } j=1,2,3\end{aligned} \quad [29]$$

where subscripts α and p refer to the active and passive phases respectively; $K_{\text{p}\alpha}{}^k$ is the partition coefficient for contaminant k from the active phase α to the passive phase p; and $K_{\text{p}\alpha}{}^k = K_{\text{aw}}{}^k$ if water is the active phase or $K_{\text{p}\alpha}{}^k = 1/K_{\text{aw}}{}^k$ if air is the active phase. Equation [29] can be put back into the form of Eq. [24] by defining effective parameters, so that the numerical solution to Eq. [29] is the same as that of Eq. [24], with effective parameters replacing the respective parameter values of Eq. [24]. These effective parameters are defined as

$$\left(D_{ij}^k\right)_{\text{eff}} = D_{ij}^k + K_{\text{p}\alpha}^k\left(D_{ij}^k\right)_{\text{p}} \quad [30]$$

$$S_{\text{eff}} = S_\alpha + K_{\text{p}\alpha}^k S_{\text{p}} \quad [31]$$

$$\left(\lambda^k S\right)_{\text{eff}} = \lambda_\alpha^k S_\alpha + \lambda_{\text{p}}^k S_{\text{p}} K_{\text{p}\alpha}^k \quad [32]$$

$$\left(\lambda^j S\right)_{\text{eff}} = \lambda_\alpha^j S_\alpha + \lambda_{\text{p}}^j S_{\text{p}} K_{\text{p}\alpha}^j \quad [33]$$

where the subscript eff denotes the effective parameter that replaces the respective parameter value in Eq. [24] during numerical solution to the transport equation. The inactive phase saturation is computed such that $S_{\text{p}} + S_\alpha = 1$. If the flow-field is transient, the saturation of the inactive phase changes along with active phase saturation changes, as a result of honoring the above constraint. While saturation changes in the active phase are balanced by the flow term computed in Eq. [1], the saturation changes in the passive phase are not. The instantaneous equilibration assumption for the passive phase does not provide the fluxes of this phase that cause phase saturation to change, and hence, neglecting this advective term in Eq. [27] and [29] omits a mass transport mechanism that would cause S_{p} to change in the storage term at any time step. Therefore, for changing S_{p} due to active phase flow, Eq. [27] and [29] are not mass-conserved equations. Options could be provided for keeping S_{p} fixed during trans-

port computations (to an initial value or a user-defined value); however, these would misrepresent the physics to maintain mass conservation. Therefore, the mass balance errors for any species should be noted for transport simulations with inactive phase partitioning in a transient unsaturated flow-field, and if large, its impact on the simulation should be examined in detail. Analysis for that species would probably be superior if conducted with the passive phase activated instead. If the assumption of neglecting passive flow advection is poor and large mass balance errors persist, it may be necessary to solve the multiphase equations with associated increased computational burden.

The additional input for transport in both air and water phases includes partitioning coefficients, diffusion coefficients for the inactive phase, and first-order decay coefficients for all species of simulation in the inactive phase.

Transport in Both Air and Water Phases with Immobile NAPL Phase

A further extension of Eq. [29] may be obtained by considering an immobile NAPL phase from which contaminant components may dissolve into water and volatize into air within the subsurface for subsequent transport, with the mass transfer process depleting NAPL phase saturations. Contaminant components may diffuse within a continuous NAPL phase, with degradation and generation of components also occurring within the NAPL phase. A mass balance equation for contaminant k in the NAPL phase may be expressed as

$$\frac{\partial}{\partial x_i}\left[\left(D_{ij}^k\right)_n \frac{\partial c_n^k}{\partial x_j}\right] = \frac{\partial}{\partial t}\left(\phi S_n c_n^k\right) + \lambda_n^k \phi S_n c_n^k - \sum_{j=1}^{\mathrm{NPAR}} \xi_{kj} \lambda_n^j \phi S_n c_n^j - \Gamma_n^k \quad [34]$$

where the subscript n denotes the NAPL phase and the term Γ_n^k is the mass transfer term for component k from the NAPL phase to the other fluid phases present. When Eq. [34] is added to Eq. [29], the term Γ_n^k cancels out, and equilibrium partitioning may be used to express NAPL phase concentrations of component k, in terms of the water phase concentration as

$$c_n^k = K_{n\mathrm{w}}^k c_{\mathrm{w}}^k \quad [35]$$

where $K_{n\mathrm{w}}^k$ is the equilibrium partitioning coefficient for contaminant k from water to NAPL. Due to equilibrium considerations, Eq. [28] may be divided by Eq. [35] to express NAPL phase concentration of component k in terms of its concentration in the air phase as

$$c_n^k = K_{n\mathrm{a}}^k c_{\mathrm{a}}^k = \frac{K_{n\mathrm{w}}^k}{K_{\mathrm{aw}}^k} c_{\mathrm{a}}^k \quad [36]$$

where K_{na}^k is the partitioning coefficient for component k from air to NAPL. Equation [34] may be added to Eq. [29], and the result may be put back in the form of Eq. [24] by defining effective parameters as

$$\left(D_{ij}^k\right)_{\mathrm{eff}} = D_{ij}^k + K_{\mathrm{p}\alpha}^k \left(D_{ij}^k\right)_{\mathrm{p}} + K_{n\alpha}^k \left(D_{ij}^k\right)_n \quad [37]$$

$$S_{\mathrm{eff}} = S_\alpha + K_{\mathrm{p}\alpha}^k S_{\mathrm{p}} + K_{n\alpha}^k S_n \quad [38]$$

$$\left(\lambda^k S\right)_{\mathrm{eff}} = \lambda_\alpha^k S_\alpha + \lambda_{\mathrm{p}}^k S_{\mathrm{p}} K_{\mathrm{p}\alpha}^k + \lambda_n^k S_n K_{n\alpha}^k \quad [39]$$

and

$$\left(\lambda^j S\right)_{\mathrm{eff}} = \lambda_\alpha^j S_\alpha + \lambda_{\mathrm{p}}^j S_{\mathrm{p}} K_{\mathrm{p}\alpha}^j + \lambda_n^j S_n K_{n\alpha}^j \quad [40]$$

where $K_{n\alpha}{}^k$ is the partitioning coefficient of component k from the active phase, α, to the NAPL phase, n. Thus, when water is the active phase we have $K_{n\alpha}{}^{\mathrm{k}} = K_{n\mathrm{w}}{}^k$ (of Eq. [35]), and when air is the active phase we have $K_{n\alpha}{}^{\mathrm{k}} = K_{n\mathrm{a}}{}^k = K_{n\mathrm{w}}{}^k / K_{\mathrm{aw}}{}^k$ (of Eq. [36]).

An operator splitting strategy is used to solve for multicomponent, multiphase transport of contaminants, with inclusion of a NAPL phase. The effective transport equation in a multiphase porous medium, discussed above, is first solved for each contaminant introduced to the subsurface via the NAPL phase. Thus, each contaminant is redistributed spatially within the domain due to mass partitioning, advection in the active phase, and multiphase dispersion, decay and generation processes. The phase-state of NAPL in the system, however, will be thrown into disequilibrium in regions where a NAPL phase exists or where it is likely to form. A flash calculation is then performed at each grid block in the region (where NAPL exists) to reset phase equilibrium conditions, as discussed below. Iterations on this scheme may be performed to avoid using extremely small time-step sizes as may be required by an operator splitting strategy that is strictly valid for explicit solution schemes, or incur large mass balance errors.

A compositional consideration is required for the NAPL phase, and all NAPL contaminant components must be included in the problem to define its equilibrium phase state. The mass of the NAPL phase is then the sum of the mass of its components giving

$$\sum_k C_n^k = \rho_n \quad [41]$$

Or alternatively, defining a mass fraction of component k in the NAPL phase, X_n^k, as the mass of k in NAPL divided by the mass of the NAPL phase, Eq. [41] gives

$$\sum_k X_n^k = 1 \quad [42]$$

By definition, we have

$$C_n^k = \rho_n X_n^k \quad [43]$$

and Eq. [41], [42], and [43] are related. The net mass of component k within a computational grid block is conserved for the flash calculation, when mass is redistributed among phases. Thus,

$$\sum_\alpha \left(\rho_\alpha S_\alpha X_\alpha^k\right)_{\mathrm{N}} = \sum_\alpha \left(\rho_\alpha S_\alpha X_\alpha^k\right)_{\mathrm{O}} \quad [44]$$

where subscript N refers to new (after flash) and subscript O refers to old (before flash) values. Equation [44] is a set of k equations for each NAPL component k. Equations [42] and [44] therefore form a set of $k + 1$ equations, which may be solved for the $k + 1$ unknowns, S_n and X_n^k for each component k, to reset equilibrium. Density for air and water required by Eq. [44] are obtained as discussed for the respective flow equations, and NAPL phase density may be obtained as a mass fraction weighted mixture of the component densities or as a mass fraction weighted mixture of component volumes. Thus,

$$\rho_n = \sum_k X_n^k \rho_n^k \quad [45]$$

or

$$1/\rho_n = \sum_k \left[X_n^k \left(\rho_n^k \right)^{-1} \right] \quad [46]$$

where ρ_n^k is the density of pure component k in its liquid state (note that $X_\alpha{}^k$ for α other than NAPL in Eq. [44] may be obtained from the equilibrium partitioning relations of Eq. [28], [35], and [36]). This set of nonlinear equations may be solved by Newton iteration, at each grid block. Solution to this set of equations is called the *flash package*, which takes the disequilibrium concentrations obtained after transporting all contaminants, and reassigns contaminant masses to the various phases present such that their concentrations are in equilibrium with an existing NAPL phase. Mass conservation is maintained; therefore, NAPL saturations change due to contaminant mass transfer in or out of the NAPL phase.

Two states of disequilibrium may occur in any grid block after the transport equations are solved for all components. First, where a NAPL phase is already present, dissolution and volatization of its components will reduce NAPL concentrations from their equilibrium constraint value of Eq. [42]. The flash package remedies this by decreasing NAPL saturations. Second, where a NAPL phase is absent, generation terms in the transport equations may create NAPL-soluble components whereby the constraints of Eq. [41] or [42] are exceeded. This is an indication of NAPL phase appearance, which will be quantified by the flash package. Where no NAPL phase exists at any time, at any location in the system, the sum of concentrations of all contaminants, as calculated for a NAPL phase, will be less than the constraint Eq. [42], and the flash routine may be skipped. Thus, as contaminants dissolve and/or volatize from the NAPL phase, the NAPL saturations reduce until no NAPL phase resides in the simulation domain. Alternatively, if NAPL-soluble components are generated, a NAPL phase may appear as determined by the flash package, which considers contaminant component mass conservation, and a compositional framework for the NAPL phase.

Additional input data required for the case of simulating multicomponent transport from an immobile NAPL phase include the NAPL–water partition coefficient, and diffusion and decay coefficients in NAPL for each component, in addition to all input required for multiphase transport discussed in the section "Transport in Both Air and Water Phases." The mass equilibration calculations of the flash package further require user input for the density of each of the NAPL components k in their pure liquid state. Furthermore, the initial NAPL saturation and composition of NAPL are also required. In addition, options are needed for interpreting the input species concentrations, for full flexibility in simulation. For the first option, the input concentrations are taken to represent active phase concentrations in equilibrium with immobile NAPL. This option is useful for restarting a simulation to continue the transients further in time, or it may be used when active phase concentrations of contaminants are known. For the second option, input concentrations are interpreted as resident NAPL phase concentrations that are in equilibrium with the other phases present. For the third option, the input concentrations are interpreted as concentration of species in the initial inventory of the in situ NAPL phase. This mass is first flashed into the other phases present (assumed initially contaminant free), before proceeding with the transport simulation. For all options, the input concentration should be consistent with constraint Eq. [42] where a NAPL phase exists. Equations [45] or [46] may then be used to determine NAPL phase density, and Eq. [43] to determine the consistent set of input values for species concentrations. Alternatively, consistency requires that sum of the mass fractions in the NAPL phase is less than unity at a node where NAPL saturation is zero. Note that analyses of systems with a mobile NAPL phase would require a multiphase or compositional simulation capability as discussed by Finsterle et al., (2008, this issue), with the associated additional nonlinearities and computational burden of simultaneously solving multiple equations per node.

Dual Domain Transport in the Unsaturated Zone

Contaminant transport behavior as expressed by Eq. [24] (or its equivalent for multiphase transport systems) misses an important significant mechanism—that of a dual domain—which produces the highly nonsigmoidal and asymmetrical distributions of tailing of contaminant noticed in several experimental studies as well as in observations of contaminant breakthrough in the field. The dual domain mechanism is significant for several conditions listed by van Genuchten and Wierenga (1976). van Genuchten (1981) showed that the same general equation applied irrespective of how the processes or mechanisms are conceptualized. Thus, the same set of dimensionless variables represents (i) linear equilibrium adsorption, physical kinetic model; (ii) physical kinetic model in presence of anion exclusion; (iii) two-site kinetic adsorption model; and (iv) one-site kinetic adsorption model. The term *dual domain* therefore represents retarding mechanisms involving both equilibrium and kinetic adsorption processes, without explicitly defining the mechanism.

Figure 2 shows some physical situations where the dual domain processes may contribute significantly to transport behavior. Figure 2a shows the situation of an aggregated soil wherein flow and advective–dispersive solute transport occur in the mobile domain, but no flow occurs in or out of the aggregated domain (soil clumps). Diffusion is the kinetic process that transfers contaminant mass in and out of the aggregates. Equilibrium adsorption onto soil grains occurs on soil within the mobile domain, as well as on soil within the aggregates. Figure 2b shows that water in dead-end regions and immediately surrounding soil grains in a porous medium is immobile. The kinetic process of diffusion transfers contaminant mass from the mobile region to the immobile region (and vice versa), from which it can adsorb (assuming equilibrium conditions) onto soil grains. Figure 2c shows a fractured medium system, for which there exists extensive literature involving the dual domain conceptualization, along with its own terminology (Brusseau et al., 1994; van Genuchten and Dalton, 1986; Huyakorn et al., 1983). Flow and advective–dispersive solute transport occur through the fracture domain, with diffusion of contaminant into the matrix. Equilibrium adsorption occurs on the soil within the matrix as well as along the fracture walls in the mobile domain. Figure 2d shows the situation wherein flow and advective–dispersive transport occurs through an extensive network of macropores, earthworm channels, or solution channels, with diffusive mass transfer into the adjacent medium. Equilibrium adsorption occurs along channel

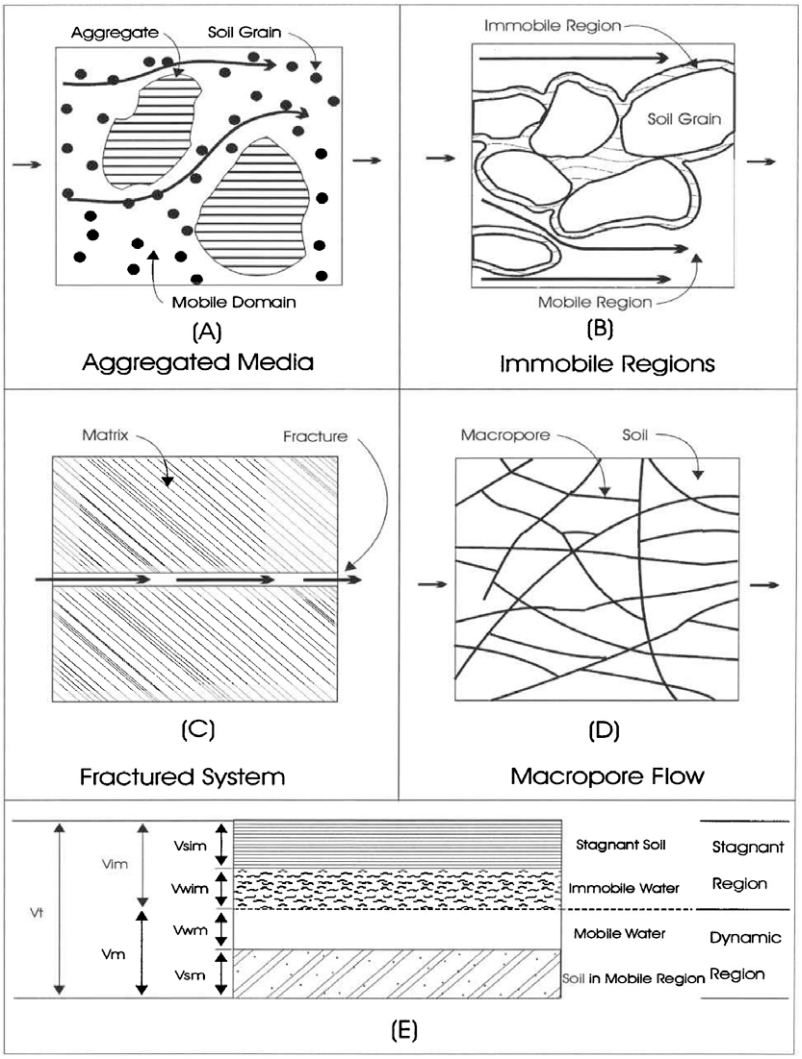

FIG. 2. Dual domain systems and conceptualization.

walls and on soil in the immobile region within the medium. Figure 2e shows the conceptual representation of all these dual region systems. Both mobile and immobile domains consist of soil and voids (filled with water and/or air). The mobile fraction, f (equivalent to fracture porosity of a dual porosity system), is the fraction of the total domain that lies in the mobile region (i.e., $f = V_m/V_T$, where V_m is the mobile domain volume and V_T is the total domain volume). The immobile fraction, $1 - f$, is therefore the ratio of the volume of the immobile domain (V_{im}) to total volume. The porosity within the mobile domain, ϕ_m, is the volume of voids in the mobile domain, V_{vm}, divided by the volume of the mobile domain, V_m. The water saturation in the mobile domain, S_{wm}, is defined by $S_{wm} = V_{wm}/V_{vm}$, where V_{wm} is the volume of water in the mobile domain. Analogously, and further assuming that the immobile domain is fully saturated with water or that the effect of air is ignored, the porosity of the immobile domain is expressed as $\phi_{im} = V_{wim}/V_{im}$, where V_{wim} is the volume of water in the immobile domain. If air is the active phase of the flow simulation, analogous definitions can be made as above, for air filled regions. The next level of analysis is that of dual permeability systems (Vogel et al., 2000, Larsbo et al., 2005) and multiple permeability systems (Gwo et al., 1995; Pruess and Narasimhan, 1985; Wu et al., 2004) where multiple flow equations are solved per node with associated jump in computational burden.

For a dual domain system, Eq. [1] describes the variably saturated transient flow of water through the mobile domain (of volume V_m) with no flow occurring into or through the immobile domain (of volume V_{im}). The equation can be cast in terms of the total system volume (from the mobile domain volume) by multiplying Eq. [1] by the mobile fraction, f, to give

$$\frac{\partial}{\partial x}\left(\mathbf{K}_{xx}k_{rw}\frac{\partial h}{\partial x}\right)+\frac{\partial}{\partial y}\left(\mathbf{K}_{yy}k_{rw}\frac{\partial h}{\partial y}\right)+\frac{\partial}{\partial z}\left(\mathbf{K}_{zz}k_{rw}\frac{\partial h}{\partial z}\right)-Wf=f\phi_m\frac{\partial S_w}{\partial t}+fS_wS_s\frac{\partial h}{\partial t} \quad [47]$$

where

$$\mathbf{K}_{ii}=fK_{ii}\quad (ii=xx,\ yy,\ \text{or}\ zz) \quad [48]$$

is the hydraulic conductivity of the total system, as may be measured by pump tests in the field, and $\mathbf{K}_{ii}$ is the conductivity of the mobile domain (e.g., conductivity of a fracture if theoretically calculated for fracture–matrix systems from fracture aperture and some flow theory such as Hagen–Poiseuille laminar flow, or conductivity of a soil sample from the mobile region outside of the aggregates if measured in the laboratory). It should be noted that the saturation S_w above denotes the saturation within the mobile region (V_{wm}/V_{vm}), and S_s is the specific storage of the (soil within the) mobile region. No water flows into or through the immobile region; thus, a flow equation for the immobile region is not required. The Darcy flux components, q_i, per unit total volume may be computed from Darcy's law as

$$q_i=\mathbf{K}_{ij}k_{rw}\frac{\partial h}{\partial x_j} \quad [49]$$

If air is the active phase in flow simulations, the above flow equations may be expressed for air instead of water as discussed earlier. For the dual domain system, the transport equation for contaminants in the active phase α within the mobile domain may be written per unit total volume as

$$\frac{\partial}{\partial x_i}\left(D_{ij}^k\frac{\partial c_m^k}{\partial x_j}\right)-\frac{\partial}{\partial x_i}\left(q_ic_m^k\right)=\frac{\partial}{\partial t}\left(f\phi_mS_{\alpha m}c_m^k\right)+\frac{\partial}{\partial t}\left(f\rho_{Bm}c_{sm}^k\right)+f\lambda_\alpha^k\phi_mS_{\alpha m}c_m^k+f\lambda_s^k\rho_{Bm}c_{sm}^k-qc_k^*+f\Gamma^k-\sum_{j=1}^{NPAR}\xi_{kj}f\lambda_\alpha^j\phi_mS_{\alpha m}c_m^j-\sum_{j=1}^{NPAR}\xi_{kj}f\lambda_s^j\rho_{Bm}c_{sm}^j+R_{m\to im}^k-R_{im\to m}^k \quad [50]$$

where f and q_i are defined above, and all terms with subscript m refer to the respective values and properties in the mobile domain. The decay rate is assumed to be the same for both immobile and mobile domains; therefore, this term is not individually subscripted. $R_{m\to im}{}^k$ is the rate of mass transfer of contaminant

k from the mobile domain to the immobile domain per unit total volume, and $R_{\mathrm{im}\rightarrow\mathrm{m}}{}^{k}$ is the mass transfer rate per unit total volume of contaminant k from the immobile to the mobile domain. Similarly, a mass balance equation for contaminant k within the immobile domain may be written per unit total volume as

$$\begin{aligned}&\frac{\partial}{\partial t}\left[(1-f)\phi_{\mathrm{im}}c_{\mathrm{im}}^{k}\right]+\frac{\partial}{\partial t}\left[(1-f)\rho_{\mathrm{Bim}}c_{\mathrm{sim}}^{k}\right]\\&+(1-f)\lambda_{\alpha}^{k}\phi_{\mathrm{im}}c_{\mathrm{im}}^{k}+(1-f)\lambda_{\mathrm{s}}^{k}\rho_{\mathrm{Bim}}c_{\mathrm{sim}}^{k}\\&-\sum_{j=1}^{\mathrm{NPAR}}\xi_{kj}(1-f)\lambda_{\alpha}^{j}\phi_{\mathrm{im}}c_{\mathrm{im}}^{j}\\&-\sum_{j=1}^{\mathrm{NPAR}}\xi_{kj}(1-f)\lambda_{\mathrm{s}}^{j}\rho_{\mathrm{Bim}}c_{\mathrm{sim}}^{j}-R_{\mathrm{m}\rightarrow\mathrm{im}}^{k}+R_{\mathrm{im}\rightarrow\mathrm{m}}^{k}=0\end{aligned}\qquad[51]$$

where it is assumed that the active phase totally occupies the void spaces within the immobile domain ($S_{\alpha\mathrm{im}} = 1$). Effective properties for ϕ_{im} and ρ_{Bim} may be used if $S_{\alpha\mathrm{im}} \neq 1$, to accommodate the inactive phase equilibrium partitioning along with equilibrium partitioning on the soil. Consistent with the assumption of no flow into or out of the immobile domain of the active phase, the immobile domain is incompressible, and ϕ_{im} and f remain constant. The rate of mass transfer from the mobile domain depends on the mobile domain concentration and is expressed by a first-order kinetic term:

$$R_{\mathrm{m}\rightarrow\mathrm{im}}^{k}=\alpha_{\mathrm{m}\rightarrow\mathrm{im}}^{k}c_{\mathrm{m}}^{k}\qquad[52]$$

where $\alpha^{k}{}_{\mathrm{m}\rightarrow\mathrm{im}}$ (T^{-1}) is the first-order kinetic rate constant. Similarly, the rate of mass transfer from the immobile domain depends on its concentration and is expressed by a first-order kinetic term as

$$R_{\mathrm{im}\rightarrow\mathrm{m}}^{k}=\alpha_{\mathrm{im}\rightarrow\mathrm{m}}^{k}c_{\mathrm{im}}^{k}\qquad[53]$$

where $\alpha^{k}{}_{\mathrm{im}\rightarrow\mathrm{m}}$ (T^{-1}) is the first-order kinetic rate constant. In Eq. [52] and [53], it is assumed that the mass transfer for each contaminant k between the two domains is not affected by the presence of the other contaminants; thus, $\alpha^{k}{}_{\mathrm{im}\rightarrow\mathrm{m}}$ and $\alpha^{k}{}_{\mathrm{m}\rightarrow\mathrm{im}}$ are constants. At equilibrium, we have $c_{\mathrm{im}}{}^{k} = c_{\mathrm{m}}{}^{k}$ and $R^{k}{}_{\mathrm{m}\rightarrow\mathrm{im}} = R^{k}{}_{\mathrm{im}\rightarrow\mathrm{m}}$; thus, $\alpha^{k}{}_{\mathrm{im}\rightarrow\mathrm{m}} = \alpha^{k}{}_{\mathrm{m}\rightarrow\mathrm{im}} = \alpha^{k}$, which is the first-order kinetic constant for mass transfer of contaminant k between domains. Equation [52] minus Eq. [53] gives

$$R_{\mathrm{m}\rightarrow\mathrm{im}}^{k}-R_{\mathrm{im}\rightarrow\mathrm{m}}^{k}=\alpha^{k}\left(c_{\mathrm{m}}^{k}-c_{\mathrm{im}}^{k}\right)\qquad[54]$$

Equation [54] may be used to replace the last two terms in Eq. [50] and [51] to give two equations in the two unknown concentrations c_{m}^{k} and c_{im}^{k} for any contaminant component k. The mass transfer rate coefficient may be related to the effective diffusivity of contaminant within the immobile domain as

$$\alpha\left(c_{\mathrm{m}}^{k}-c_{\mathrm{im}}^{k}\right)=D_{\mathrm{im}}^{*}\frac{\partial c_{\mathrm{im}}}{\partial\chi}(1-f)\sigma\qquad[55]$$

where $D_{\mathrm{im}}{}^{*}$ is the effective diffusion coefficient (inclusive of tortuosity) within the immobile domain, χ is the length dimension within the immobile domain, and α is the specific surface between the two domains defined as the area of contact divided by the volume of the immobile domain. In Eq. [55], it is assumed that diffusion into the immobile domain is the rate controlling process and that processes at the interface of the two domains are relatively fast. Equation [55] can be simplified to algebraic relations for various geometry matrix blocks, including spherical, rectangular slabs, and others (van Genuchten and Dalton, 1986). These relations may be used to estimate α as a function of $D_{\mathrm{im}}{}^{*}$ and matrix-block dimensions when field data is lacking.

The flow equation for the dual domain system is identical to that of the single continuum representation, with the right-hand side of Eq. [1] containing the mobile fraction, f, which may be multiplied into the primary and secondary storage terms immediately after they are read. The transport Eq. [50] and [51], with Eq. [54] providing the mass transfer term, are discretized into two equations in two unknowns (for each component), c_{m}^{k} and c_{im}^{k}, where the concentrations are expressed for the active phase (note that c_{sm}^{k} and c_{sim}^{k} may be obtained from the equilibrium Freundlich isotherms for the two domains, and concentrations in the other phases that are present, may be obtained from equilibrium partitioning). In general, the discretized transport equations within the two domains may be represented as

$$\mathbf{A}_{1}^{k}\mathbf{c}^{k}+\mathbf{B}_{1}^{k}\mathbf{c}_{\mathrm{im}}^{k}=\mathbf{R}_{1}^{k}\qquad[56]$$

$$\mathbf{A}_{2}^{k}\mathbf{c}^{k}+\mathbf{B}_{2}^{k}\mathbf{c}_{\mathrm{im}}^{k}=\mathbf{R}_{2}^{k}\qquad[57]$$

where $\mathbf{B}_{1}{}^{k}$, $\mathbf{A}_{2}{}^{k}$, and $\mathbf{B}_{2}{}^{k}$ are diagonal matrices since there is no flow in the immobile domain, and $\mathbf{c}^{k}$ (= $\mathbf{c}_{\mathrm{m}}^{k}$) represents the concentration in the mobile domain. Manipulating Eq. [57] gives

$$\mathbf{c}_{\mathrm{im}}^{k}=\frac{\mathbf{R}_{2}^{k}}{\mathbf{B}_{2}^{k}}-\frac{\mathbf{A}_{2}^{k}}{\mathbf{B}_{2}^{k}}c^{k}\qquad[58]$$

which may be inserted into Eq. [56] to give

$$\left[\mathbf{A}_{1}^{k}-\frac{\mathbf{A}_{2}^{k}}{\mathbf{B}_{2}^{k}}\right]\mathbf{c}^{k}=\left[\mathbf{R}_{1}^{k}-\frac{\mathbf{R}_{2}^{k}}{\mathbf{B}_{2}^{k}}\mathbf{B}_{1}^{k}\right]\qquad[59]$$

The matrix and right-hand-side vector of the basic transport routines may be manipulated according to Eq. [59] before each solve for $\mathbf{c}^{k}$ (at any time step or iteration). $\mathbf{c}_{\mathrm{im}}{}^{k}$ may then be obtained from back substitution of the calculated $\mathbf{c}^{k}$ into Eq. [58]. Thus, the matrix equation still solves one equation per computational grid block for $\mathbf{c}_{\mathrm{m}}^{k}$, with $\mathbf{c}_{\mathrm{im}}^{k}$ being obtained in a single forward substitution–backward elimination process. This simultaneous solution scheme is advantageous over operator splitting, which may approximate the effect of one domain on the other by time-lagging the solutions to Eq. [56] and [57] or require a larger computational burden by iterating over the equations till convergence. The second term of Eq. [51] is expanded using the modified-Picard method due to the nonlinear retardation term, as is done for the second term on the right-hand side of Eq. [50] for the mobile domain.

The dual domain system requires additional input to define the two domains. First, the fraction of the total domain occupied by the mobile domain, f, is required as additional input. Further, the mass transfer rate term α, the porosity ϕ_{im}, adsorption parameters K_{im}^{k} (and $\eta_{\mathrm{im}}{}^{k}$ for nonlinear cases), and initial concentrations of each component k, within the immobile domain are also required as input. Additional output for dual domain simulations includes concentrations of the contaminants in the active phase

within the immobile region, the mass balance components of storage, decay, and generation of contaminants in the immobile domain, and the mass transfer between domains. Note that the dual domain concept is applied to the transport equation only. Dual porosity unsaturated flow is, however, represented by use of Eq. [4] to characterize the multiple permeability domains in the Richards equation.

Simulation of Complex Reactions

In certain cases, subsurface transport of contaminants may not be adequately characterized using first-order chain (sequential) decay reactions, and complex interactions between contaminants may need to be quantified. MODFLOW SURFACT has included the SALTCHEM module of the UNSATCHEM software package (Šimůnek et al., 1996) to include capability of major ion equilibrium and kinetic chemistry. The UNSATCHEM module is a complex reaction package developed by other researchers, and similar modules can be accommodated within MODFLOW SURFACT by compiling them as dynamic link libraries that will work seamlessly with the code. In addition, MODFLOW SURFACT includes the reaction package of the RT3D code which is another complex reaction package for biodegradataion developed by other researchers (Clement, 1997). The RT3D capabilities are further expanded to accommodate unsaturated conditions with possible presence of immobile NAPL. The RT3D code contains several common environmental reactions of interest, including instantaneous aerobic decay of benzene, toluene, ethylbenzene, and xylene (BTEX); instantaneous decay of BTEX using multiple electron acceptors; kinetic limited decay of BTEX using multiple electron acceptors; and double Monod model for interactions between hydrocarbon, electron acceptor, and bacterial cells. Further, RT3D accommodates user defined reactions whereby the user provides only the functional form of the desired reactions which are solved by the ODE solver within the RT3D framework.

Solution to reactive transport is obtained using an operator splitting approach whereby the SALTCHEM or modified RT3D reaction package performs the reaction calculations while MODFLOW SURFACT performs the transport calculations. Additional input required for use of the SALTCHEM or RT3D modules includes the reaction rates and stoichiometry within all phases (water, NAPL, air, and soil).

Numerical Solution of Flow Equations

The governing flow equations of MODFLOW SURFACT discussed above solve one equation per numerical grid block to achieve a wide range of simulation capabilities, including unconfined flow (Eq. [1] with GSVE considerations), unsaturated flow (Eq. [1]), flow through wells (Eq. [5]), and flow of air (Eq. [15]), to evaluate a wide range of environmental problems and remedial alternatives at varying levels of complexity. This avoids the numerical burden of simultaneously solving multiple equations per grid block as required by multiphase or compositional models. This equation, however, can be highly nonlinear for the various applications of the vadose zone equation within the code. Numerically robust and efficient schemes suitable for highly nonlinear equations are therefore necessary to solve the governing flow equations.

An important consideration in time-marching schemes for transient nonlinear simulations is the use of adaptive time stepping. The adaptive time stepping scheme presented here is simple and effective and is adapted from Kool and van Genuchten (1991). The scheme increases the time-step size by a user-prescribed factor (up to a prescribed maximum) when convergence is easy, reduces the time-step size by another user-prescribed factor when convergence is hard, and cuts the time-step size to reattempt solution after failed iterations. Adaptive time stepping is necessary to achieve efficiency and robustness in solving highly nonlinear problems. A further consideration when using adaptive time stepping is to adapt time-step sizes to also honor user-prescribed time values at which output is required and to honor time values when boundary conditions are changed.

Nonlinear equations are often solved by using the Picard iteration scheme or its variants. For highly nonlinear situations, the Picard scheme requires small time-steps and several iterations for solution to practical problems. Further, for steady-state simulations, the Picard scheme may fail altogether. The Newton–Raphson linearization scheme is well suited for highly nonlinear problems as encountered in environmental flow situations. Newton–Raphson linearization provides quadratic convergence and can greatly alleviate convergence difficulties. In addition, a backtracking algorithm is implemented to stabilize the Newton iterations and an under-relaxation technique alleviates oscillatory behavior for robust and efficient simulations.

An implicit time discretization of the vadose zone flow (Eq. [1]) can be expressed in matrix form as

$$\left(\frac{\mathbf{B}^{k+1}}{\Delta t}+\mathbf{A}^{k+1}\right)\mathbf{h}^{k+1}=\mathbf{F}^{k+1}+\frac{\mathbf{B}^{k+1}}{\Delta t}\mathbf{h}^{k} \qquad [60]$$

where superscripts $k + 1$ and k denote current and previous time levels respectively, Δt is the time-step size, $\mathbf{B}$ is a diagonal storage matrix, $\mathbf{A}$ is the flux matrix, $\mathbf{h}$ the potentiometric head, and $\mathbf{F}$ is an external flux. The storage term of Eq. [60] is assembled using the modified Picard scheme of Celia et al. (1990). The modified Picard scheme in effect applies a Newton-type linearization to the storage term, so additional consideration is only required for Newton–Raphson linearization of the flow terms, $\mathbf{A}^{k+1}$, of Eq. [60]. This can be expressed as (Huyakorn and Pinder, 1983)

$$\mathbf{A}^{r+1}=\mathbf{A}^{r}+\left(\frac{\partial\mathbf{A}}{\partial\mathbf{h}}\right)^{r}\Delta\mathbf{h}^{r+1}=0 \qquad [61]$$

where r and $r + 1$ denote previous and present iteration levels at the current time value and $\Delta\mathbf{h}^{r+1}$ is the iteration displacement vector or update vector expressed as

$$\Delta\mathbf{h}^{r+1}=\mathbf{h}^{k+1}-\mathbf{h}^{r} \qquad [62]$$

Substituting Eq. [62] in Eq. [6] and rearranging yields the Newton expansion for the flow term as

$$\mathbf{H}^{r}\mathbf{h}^{k+1}=\mathbf{H}^{r}\mathbf{h}^{r}-\mathbf{A}^{r} \qquad [63]$$

where

$$\mathbf{H}^{r}=\left(\frac{\partial\mathbf{A}}{\partial\mathbf{h}}\right)^{r} \qquad [64]$$

which may be expanded for each row of the matrix as

$$\mathbf{H}_i^r = \mathbf{A}_{ij} + \sum_{k=1}^{N} \frac{\partial \mathbf{A}_{ik}}{\partial \mathbf{h}_j} \mathbf{h}_k \quad [65]$$

where the summation is over all N neighboring flow connections to node i including node i itself. The left-hand-side matrix of Eq. [60] is symmetric. The modified Picard method applies a Newton type linearization on the storage term that is only on the diagonal; therefore, the matrix remains symmetric. The additional terms of Eq. [65], however, create an asymmetric system of equations that are not compatible with the solvers that exist in the USGS releases of MODFLOW. Therefore, a solution to $\mathbf{h}^{k+1}$ is sought for this asymmetric system using an Orthomin solution scheme (Behie and Vinsome, 1982; Panday et al., 1993). The Orthomin scheme is a preconditioned conjugate gradient-type solution method that is applicable to asymmetric matrices. It consists of a preconditioning step (level-based ILU decomposition is used) and the Orthomin acceleration step, which minimizes the norm of the residual over orthogonal direction vectors. Note that this solver is also used by the transport routines, and hence the matrix structure can be shared.

Full Newton iterations may diverge for many situations, and techniques are applied to stabilize the solution process. Oscillatory behavior in solution is dampened by using the under-relaxation formula of Cooley (1983). The solution is further stabilized by using a backtracking formula. After each solution for $\mathbf{h}^{k+1}$, the $L_{\bar{2}}$ norm residual of Eq. [60] is calculated. If this residual is larger than a factor of RESRED from the value at the previous iteration, the update vector for the current iteration is shortened by a factor of BFACT (note that 0 < BFACT < 1). This process is repeated until the residual of the current iteration is within RESRED times its value at the previous iteration, before proceeding to the next Newton iteration. Strict residual reduction may be enforced by setting RESRED to ≤ 1. Larger values of RESRED allow the residual to increase between iterations and are useful to jump out of local minima during solution. Although additional computational effort is required per iteration in implementing Newton–Raphson linearization with backtracking, experience has indicated its robustness to prove more computationally efficient in solving highly nonlinear problems.

Numerical Solution of the Transport Equations

The transport modules follow the same convention for spatial and temporal discretizations as that used by the flow modules. Using the cell index terminology, the finite-difference equation for a cell i, j, k may be written in the form

$$\begin{aligned}
&\nabla_x\left(\tau_{xx}^k \nabla_x \hat{c}^k\right) + \nabla_y\left(\tau_{yy}^k \nabla_y \hat{c}^k\right) + \nabla_z\left(\tau_{zz}^k \nabla_z \hat{c}^k\right) \\
&- \nabla_x\left(Q_x \hat{c}^k\right) - \nabla_y\left(Q_y \hat{c}^k\right) - \nabla_z\left(Q_z \hat{c}^k\right) = \left(\Delta x_j \Delta y_i \Delta z_k\right) \\
&\left\{\nabla_t\left(\phi S_w c^k\right) + \nabla_t\left(\rho_B c_s^k\right) + \left(\lambda_w^k \phi S_w c^k + \lambda_s^k \rho_B c_s^k\right.\right. \\
&\left.\left. - \sum_{j=1}^{\mathrm{NPAR}} \xi_{kj} \lambda_s^j \rho_B c_s^j - \sum_{j=1}^{\mathrm{NPAR}} \xi_{kj} \lambda_w^j \phi S_w c^j\right)^{n+1}\right\} - \left(Q c^{k*}\right)^{n+1} \quad [66] \\
&+ \nabla_x\left(\tau_{xy}^k \nabla_y \hat{c}^k\right) + \nabla_x\left(\tau_{xz}^k \nabla_z \hat{c}^k\right) + \nabla_y\left(\tau_{yx}^k \nabla_x \hat{c}^k\right) \\
&+ \nabla_y\left(\tau_{yz}^k \nabla_z \hat{c}^k\right) + \nabla_z\left(\tau_{zx}^k \nabla_x \hat{c}^k\right) + \nabla_z\left(\tau_{zy}^k \nabla_y \hat{c}^k\right)
\end{aligned}$$

where $\hat{c}^k$ is the time-weighted concentration for component k; ∇_x, ∇_y, and ∇_z are finite-difference gradient operators in the x, y, and z directions, respectively; ∇_t is the temporal difference operator; $n + 1$ denotes the current time level; τ_{xx}, τ_{yy}, τ_{zz} are the discretized dispersive terms; and Q_x, Q_y, Q_z are the volumetric fluxes in the principal coordinate directions. The discretized cross dispersion terms, τ_{xy}, τ_{xz}, τ_{yx}, τ_{yz}, τ_{zx} and τ_{zy}, can optionally be taken into account by iterative updating. Calculation of all dispersion coefficients at interblock locations are performed by accounting for variable cell thickness as detailed by Zheng (1990). The time-averaged concentration for each component k may be written as

$$\hat{c}^k = \theta\left(c^k\right)^{n+1} + (1-\theta)\left(c^k\right)^n \quad [67]$$

where n is the previous time level, $n + 1$ is the current time step, and θ is the Crank–Nicolson factor, which is unity for fully implicit, 0.5 for Crank–Nicolson, and 0 for fully explicit time discretization.

The interblock concentration in the advection terms on the left-hand side of Eq. [66] are calculated using a mass conservative second-order total variation diminishing (TVD) scheme (Harten, 1983; Blunt and Rubin, 1992; Forsyth, 1994; Unger et al., 1996) with the van Leer flux limiter (van Leer, 1977, 1979). Expansion of the interblock advective flux term may be written as

$$\nabla_i\left(Q_i \hat{c}^k\right) = Q_{i+1/2} \hat{c}_{i+1/2}^k - Q_{i-1/2} \hat{c}_{i-1/2}^k \quad [68]$$

where i is any coordinate direction (i = 1,2,3), $i + 1/2$ is the forward face of the grid block, and $i - 1/2$ is the backward face of the grid block in the ith coordinate direction. The concentration at the face $\hat{c}_{i+1/2}^k$ may be expressed in a TVD form as

$$\hat{c}_{i+1/2}^k = \hat{c}_{\mathrm{ups}}^k + \sigma\left(\gamma_{ij}\right)\left(\frac{\hat{c}_{\mathrm{dwn}}^k - \hat{c}_{\mathrm{ups}}^k}{2}\right) \quad [69]$$

where "ups" is the upstream point and "dwn" is the downstream point of the nodal pair i and $i + 1$, and σ is the flux limiter term, which is a function of γ_{ij}, the smoothness sensor. Concentration at the face $\hat{c}_{i-1/2}^k$ is expressed in a similar fashion. The smoothness sensor for the concentration front γ_{ij}, is defined by

$$\gamma_{ij} = \left(\frac{\hat{c}_i^k - \hat{c}_{i2\mathrm{up}}^k}{\hat{c}_j^k - \hat{c}_i^k}\right) \quad \text{if } i = \mathrm{ups}(i,j) \quad [70a]$$

or

$$\gamma_{ij} = \left(\frac{\hat{c}_j^k - \hat{c}_{j2\mathrm{up}}^k}{\hat{c}_i^k - \hat{c}_j^k}\right) \quad \text{if } j = \mathrm{ups}(i,j) \quad [70b]$$

where i2up or j2up is the second upstream point of the pair i,j. The van Leer flux limiter is written as

$$\begin{aligned}
\sigma\left(\gamma_{ij}\right) &= 0 \qquad \text{if } \gamma_{ij} \leq 0 \\
&= \frac{2\gamma_{ij}}{1+\gamma_{ij}} \quad \text{if } \gamma_{ij} > 0
\end{aligned} \quad [71]$$

The TVD scheme minimizes numerical dispersion and preserves monotonicity properties of the exact solution and appears in Eq. [69] as a correction to the upstream solution. The smoothness sensor is calculated from concentrations at the downstream, upstream, and second point upstream nodes and detects rapid

changes in concentration. The van Leer flux limiter weights the solution from fully upstream to fully downstream. When the degree of implicitness of the solution varies, the Crank-Nicolson factor is chosen as close to 1/2 as possible without violating the TVD property of the solution (Blunt and Rubin, 1992).

The TVD property applied to the advective term ensures physically correct solutions without spurious oscillations even for totally advective transport. As stated by Harten (1983), the TVD property guarantees that for a nonlinear, scalar equation or a linear system of equations, the total variation (TV) of the solution will not increase as the solution advances in time; that is,

$$\mathrm{TV}\left(c^{n+1}\right) \leq \mathrm{TV}\left(c^{n}\right) \quad [72]$$

where $n + 1$ and n denote the current and previous time levels, and the total variation of a quantity c is defined as

$$\mathrm{TV}(c) = \sum_{i=1}^{N} \left| c_i - c_{i-1} \right| \quad [73]$$

in which i and $i - 1$ denote adjacent grid points and the sum is over the entire domain.

Nonlinearities in adsorption or of implicit TVD schemes used to solve the transport equation are treated using modified Picard iterations as per Huang et al. (1998). The Cooley (1983) under-relaxation scheme may be used to dampen flip-flop behavior during iterations. The system of matrix equations is solved using the Orthomin scheme (Behie and Vinsome, 1982; Panday et al., 1993).

Verification Problems

The various flow and transport routines were verified against analytical solutions as well as solutions from other numerical codes. Table 1 lists comparisons with analytical solutions and Table 2 lists comparisons with other numerical solutions used for verifying the code. For all examples, the MODFLOW SURFACT results compare very well with the respective analytical and numerical counterparts.

Example Applications

Two examples are provided here to demonstrate the use of the unsaturated zone flow and transport equations in providing a wide variety of analyses as needed for site investigations. The first problem demonstrates how NAPL remedial investigations may be conducted using MODFLOW SURFACT instead of complex multiphase compositional models with significantly larger computational burden. The second problem demonstrates the significance of appropriate parameterization of fractured systems for contaminant transport and remediation.

Problem 1: Examination of DNAPL Remediation

This problem examines migration of dissolved and volatilized perchloroethylene (PCE) and its degradation products from an immobile dense nonaqueous phase liquid (DNAPL) source within the subsurface. A two-dimensional cross-section of the domain, shown in Fig. 3, is simulated to study the effects of waterflooding and air-sparging remedial technologies. The domain is 20 by 1 by 5 m in the x, y, and z dimensions and is discretized using 20 by 1 by 10 cells of dimension 1 by 1 by 0.5 m. Ambient flow of water occurs under a hydraulic head of 3 m at the upstream boundary and 2.9 m at the downstream boundary. Dense nonaqueous phase liquid, initially containing PCE entirely, is located within the cross-section with saturations ranging from 0.1 to 0.3 as shown in Fig. 3. This initial mass of contaminant is flashed into all phases of the system at the start of the simulation. The initial PCE is assumed to biodegrade to trichloroethylene (TCE), dichloroethylene (DCE), and vinyl chloride (VC), with the same degradation rates in air, water, NAPL, and soil. Physical properties of the porous medium are shown in Table 3, and chemical properties of the contaminants are shown in Table 4.

The first simulation considers the ambient case in which dissolved PCE and its degradation products migrate with advection

Table 1. Benchmark problems for MODFLOW SURFACT with analytical solutions.

Problem	Description	Reference	Comment
1	Well pumping in an unconfined aquifer subject to delayed yield effects.	Neuman (1972)	Used to test new unconfined flow routines and adaptive time-stepping scheme.
2	Theis solution for pumping in an unconfined aquifer.	Theis (1935)	Used to test unconfined flow routines and fracture well routines.
3	Papadopoulos and Cooper solution for pumping in an unconfined aquifer with wellbore storage effects.	Papadopoulos and Cooper (1967)	Used to test unconfined flow routines and fracture–well routines with wellbore storage.
4	Flow to parallel drains in an unconfined aquifer.	Bear (1979)	Used to test unconfined flow routines and recharge-seepage face development.
5	Seepage through a square embankment.	Cooley (1983)	Used to test unconfined flow routines and recharge-seepage face development.
6	Two-dimensional transport due to (a) injection or withdrawal well, (b) point source, and (c) injection and withdrawal well pair.	(a) Gelhar and Collins (1971), (b) Wilson and Miller (1978), (c) Hoopes and Harleman (1967)	Used to test transport routines in multiple dimensions.
7	One-dimensional, single species transport.	Ogata and Banks (1961) or Bear (1979)	Used to test accuracy and stability of transport routines for various dispersivities, including a zero value for dispersivity.
8	One-dimensional transport of a three-member radioactive decay chain.	Coats and Smith (1964) or Lester et al. (1975)	Used to test chain decay transport routines.
9	Vertical one-dimensional air flow in a single-layer soil bounded below by the groundwater table.	Shan (1995)	Used to test air flow and density variation effects on the unsaturated zone air flow solution.

Table 2. Benchmark problems for MODFLOW SURFACT with published numerical solutions.

Problem	Description	Reference	Comment
1	Transient infiltration in an unsaturated vertical soil column.	Huang et al. (1996)	Demonstrates unsaturated flow solution for extremely dry conditions. Also tests Newton–Raphson linearization module.
2	Two-dimensional cross-sectional flow and transport in an unsaturated soil slab.	Huyakorn et al. (1985)	Tests unsaturated flow and transport solutions in multidimensions. Also tests Newton–Raphson linearization module.
3	Three-dimensional air phase flow simulation study for a field site.	Panday et al. (1994)	Tests single-phase air flow assumptions against multiphase flow results. Also compares with field observations.
4	Three-dimensional unconfined flow under a waste disposal site.	Jones and Gibbs (1995), Porter et al. (2000)	Tests Newton–Raphson linearization module. Picard scheme does not converge for a one-step steady-state solution of this problem.
5	Active water phase transport with mass transfer and diffusion in inactive air phase.	Inhouse documentation: HydroGeoLogic (1998)	Tests multiphase transport routines against a sophisticated, finite-element, multiphase flow and transport code.
6	Flash a three-phase closed system into equilibrium.	Inhouse documentation: HydroGeoLogic (1998)	Tests flash package for calculating equilibrium saturations and mole/mass fractions from a given disequilibrium state (simple mass balance).
7	Longitudinal transport in fractures with transverse matrix diffusion.	van Genuchten and Wierenga (1976)	Tests dual domain transport routines.
8	One-dimensional transport of a three-member radioactive decay chain.	Coats and Smith (1964) or Lester et al. (1975)	Demonstrates "user-defined" complex reactions solution module. This module was used to read in chain decay functions to also test their efficiency and robustness versus direct solution for chain decay.

Table 3. Physical properties of soil for dense nonaqueous phase liquid remediation example.

Property†	Value
Hydraulic conductivity	
$K_x = K_y = K_z$	1.0 m d^{-1}
Porosity	
ϕ	0.25
Dispersivity	
α_L	0.5 m
α_{TH}	0.05 m
α_{TV}	0.005 m
Mass density of soil	
ρ_B	1,600 kg m^{-3}
van Genuchten parameters	
α	5.0 m^{-1}
β	1.9
S_{wr}	0.2

† α_L, longitudinal dispersivity; α_{TH}, transverse horizontal dispersivity; α_{TV}, transverse vertical dispersivity S_{wr}, residual water saturation.

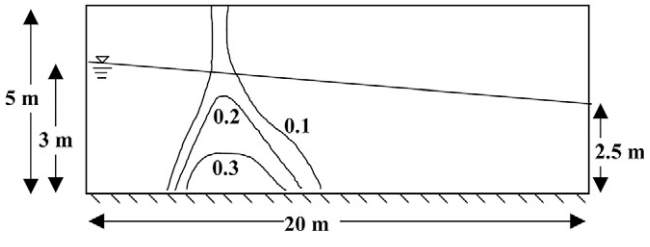

Fig. 3. Schematic diagram for dense nonaqueous phase liquid remediation example.

Table 4. Chemical properties of contaminants for dense nonaqueous phase liquid remediation example.

Property†	Value
Diffusion coefficient in water phase	
$Dw_{PCE} = Dw_{TCE} = Dw_{DCE} = Dw_{VC}$	1×10^{-5} m^2 d^{-1}
Diffusion coefficient in air phase	
$Da_{PCE} = Da_{TCE} = Da_{DCE} = Da_{VC}$	1×10^{-4} m^2 d^{-1}
Diffusion coefficient in NAPL	
$Dn_{PCE} = Dn_{TCE} = Dn_{DCE} = Dn_{VC}$	1×10^{-5} m^2 d^{-1}
Gas–water partitioning coefficient	
Kgw_{PCE}	0.9043
Kgw_{TCE}	0.0835
Kgw_{DCE}	0.1053
Kgw_{VC}	0.1222
NAPL–water partitioning coefficient	
Knw_{PCE}	6792.0
Knw_{TCE}	1028.0
Knw_{DCE}	404.0
Knw_{VC}	329.0
Decay coefficient in water, air, NAPL, and soil	
λ_{PCE}	4.747×10^{-4} d^{-1}
λ_{TCE}	4.747×10^{-4} d^{-1}
λ_{DCE}	6.330×10^{-4} d^{-1}
λ_{VC}	9.493×10^{-4} d^{-1}
Soil–water partitioning coefficient	
Kd_{PCE}	1.82×10^{-3} m^3 kg^{-1}
Kd_{TCE}	6.30×10^{-4} m^3 kg^{-1}
Kd_{DCE}	3.25×10^{-4} m^3 kg^{-1}
Kd_{VC}	1.49×10^{-4} m^3 kg^{-1}
Standard mass density of contaminant	
ρ_{PCE}	1630.0 kg m^{-3}
ρ_{TCE}	1440.0 kg m^{-3}
ρ_{DCE}	1220.0 kg m^{-3}
ρ_{VC}	908.0 kg m^{-3}

† DCE, dichloroethylene; NAPL, nonaqueous phase liquid; PCE, perchloroethylene; TCE, trichloroethylene; VC, vinyl chloride.

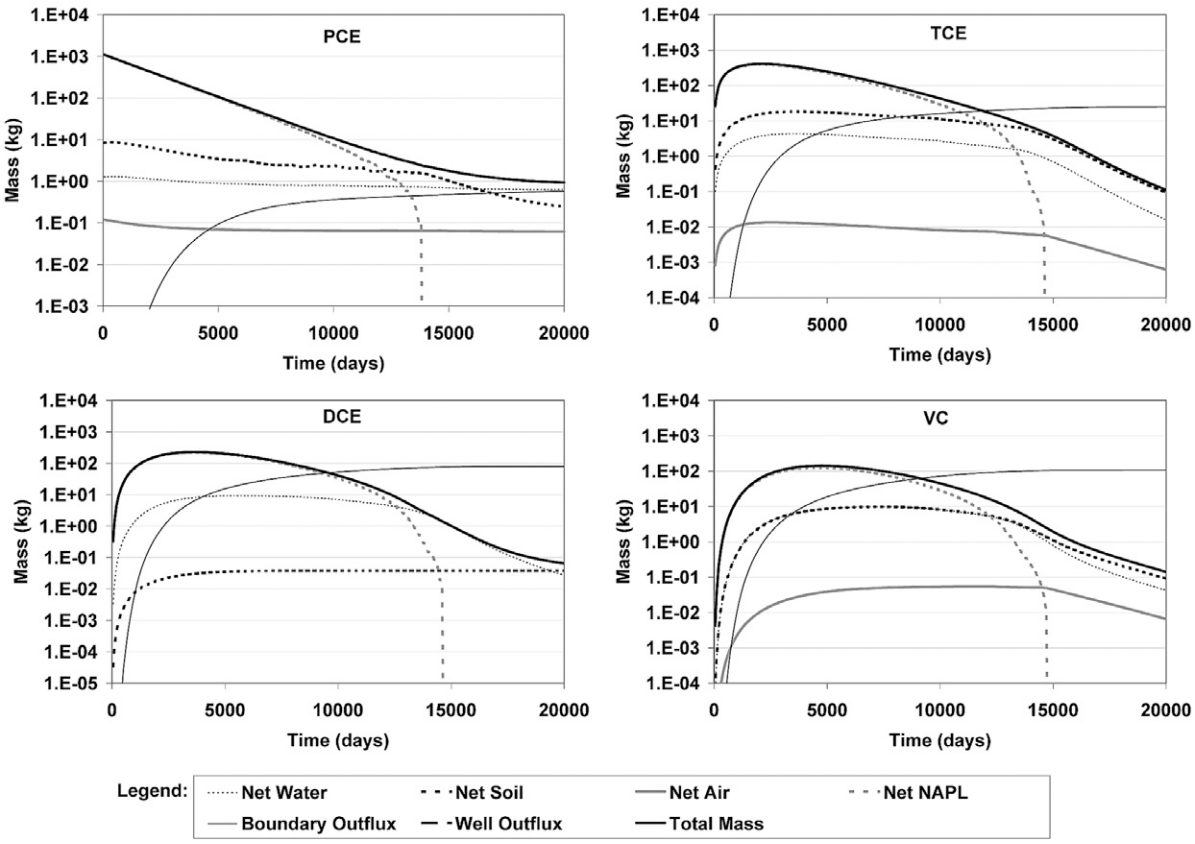

FIG. 4. Mass budgets for perchloroethylene (PCE), trichloroethylene (TCE), dichloroethylene (DCE), and vinyl chloride (VC) for a case of dense nonaqueous phase liquid remediation under ambient conditions. NAPL, nonaqueous phase liquid.

and dispersion in the groundwater flow field, and with volatilization and diffusive movement in the air phase above the water table. Figure 4 shows the mass balance components of PCE, TCE, DCE, and VC with time. Total mass of PCE decreases due to degradation and flow out the downstream end. Perchloroethylene mass in water, soil, and air phases increase almost immediately to their maximum values due to partitioning from the NAPL, then gradually decrease as the NAPL mass reduces and as PCE biodegrades. Mass of TCE, DCE, and VC in all phases increases rapidly due to sequential degradation and then gradually decreases as mass exits the downstream boundary. When NAPL disappears by about 14,500 d, mass of all components starts to decrease as the system cleans itself out through the downstream boundary.

The second simulation considers placing an extraction well downstream of the NAPL region, to capture all contaminants before they reach the compliance point along the downstream boundary. This well is placed 14.5 m downstream of the left edge of the cross-section, and pumps a total of 3 $m^3\ d^{-1}$. Figure 5 shows the mass balance components of PCE, TCE, DCE, and VC with time for this scenario. The curves for total mass of the contaminants, and masses in the respective phases, are similar to those of the ambient case (Fig. 4), with a much more rapid response in the first 6000 d, when the NAPL beneath the water table is aggressively cleaned up. The NAPL components persist in the unsaturated zone since diffusion in air and water are the only mechanisms of transport, with decay being the only attenuating factor therein. No mass is lost through the downstream boundary, hence keeping the compliance point entirely free of contaminants, with mass leaving the domain through the remediation well.

The third simulation considers reducing the pumping rate at the extraction well to 0.02 $m^3\ d^{-1}$. Figure 6 shows the mass balance components of PCE, TCE, DCE, and VC with time for this case. The curves are more similar to those of the ambient case (Fig. 4) than the high pumping case (Fig. 5). Additional observations of the simulation indicate that PCE mass does not reach the compliance point at the downstream boundary, since it decays or is captured by the well. Masses of TCE, DCE, and VC, however, do reach the downstream boundary, with concentrations as high as 0.04 mg L^{-1} for these compounds. The well, however, captures at least 100 times more mass than passes the downstream boundary for any contaminant component.

A fourth simulation considers the same reduced pumping rate at the extraction well (of 0.02 $m^3\ d^{-1}$), with an injection of all the treated pumped water 3 m downgradient from the pumping location, in an attempt to create a hydraulic barrier. The mass balance components of PCE, TCE, DCE, and VC with time are similar to Fig. 6 for this case. Additional observations of the simulation indicate that concentrations of components leaving the downstream boundary are less than 0.01 mg L^{-1} due to dilution in the injected water, even though mass leaving the downstream boundary is about the same as for the ambient case. The injection well therefore is not an effective hydraulic barrier; however, dilution effects help achieve compliance by reducing concentrations at the downstream boundary. Larger injection rates (0.08 $m^3\ d^{-1}$) do cause barrier effects with less mass leaving the downstream boundary; however, this causes the water levels to rise in the vicinity of the injection well by as much as 1 m, which may not be desirable from some ecological standpoint.

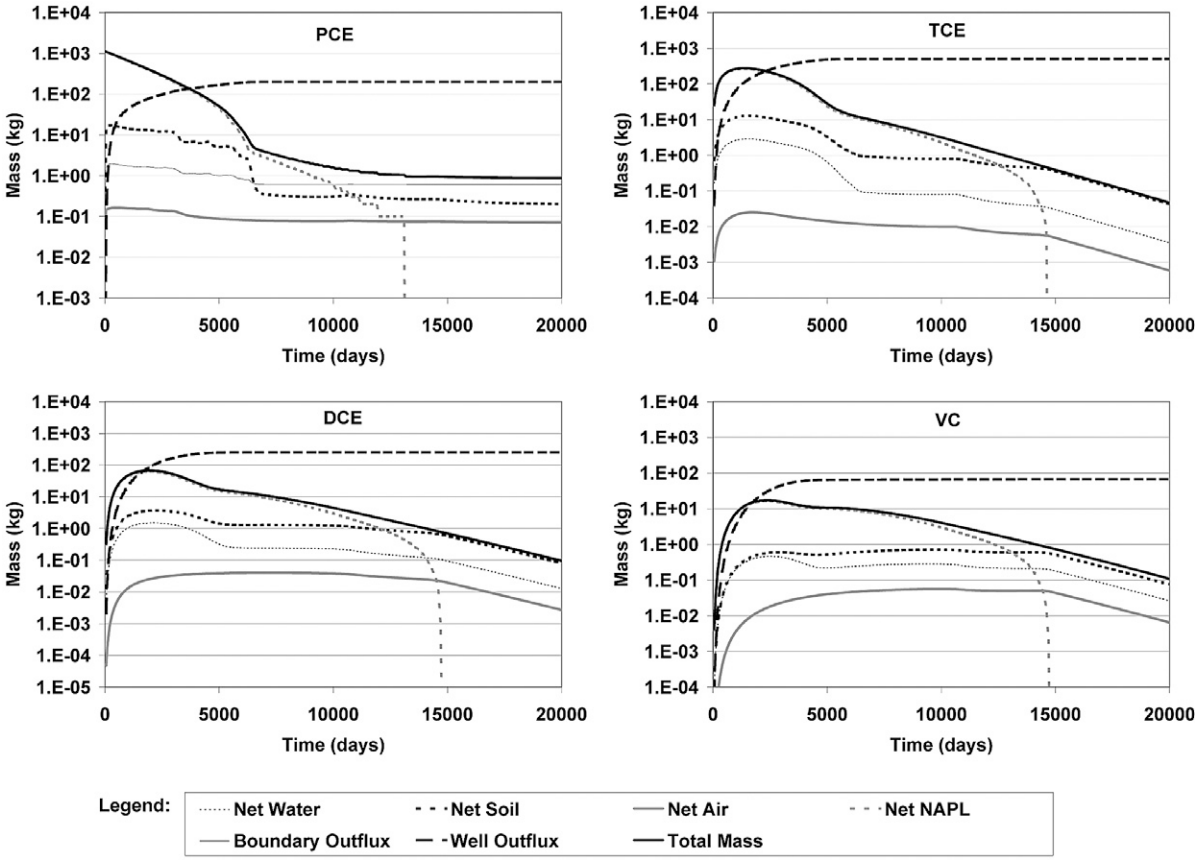

FIG. 5. Mass budgets for perchloroethylene (PCE), trichloroethylene (TCE), dichloroethylene (DCE), and vinyl chloride (VC) for a case of dense nonaqueous phase liquid remediation under high pumping conditions. NAPL, nonaqueous phase liquid.

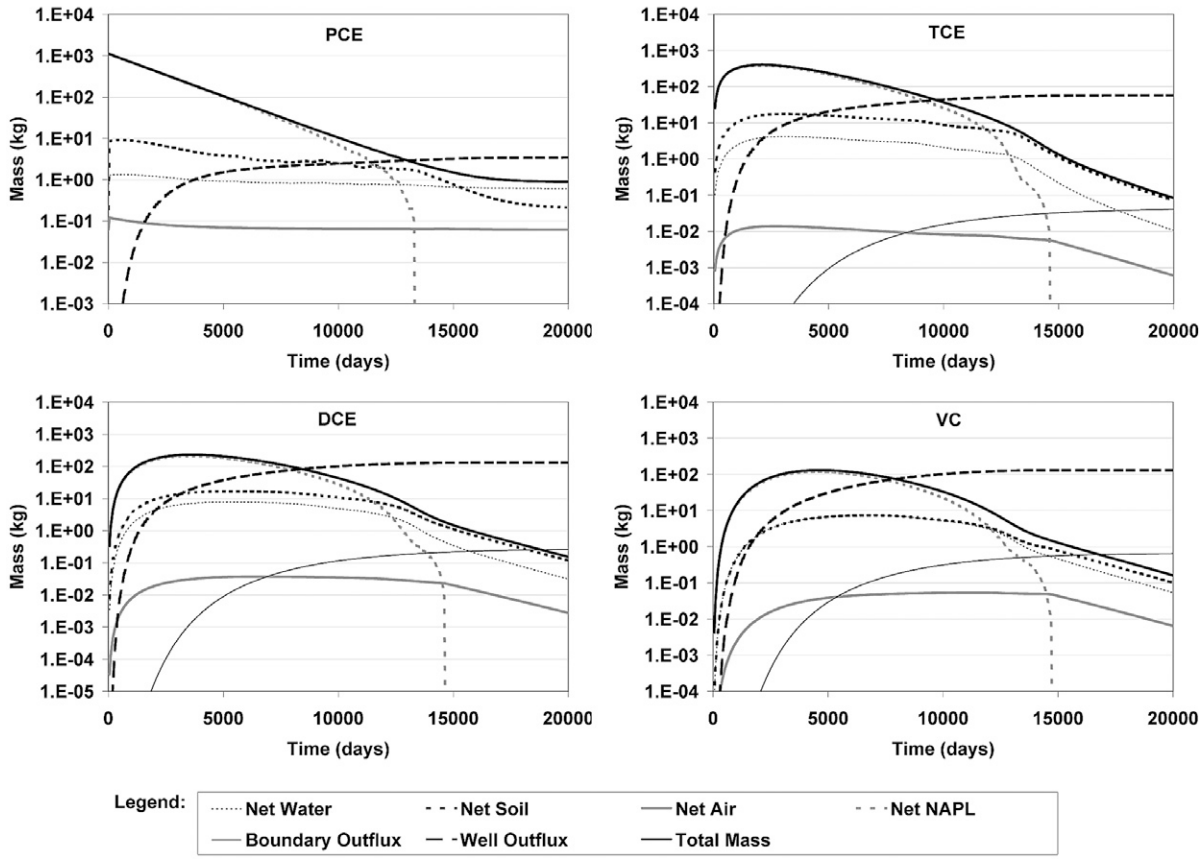

FIG. 6. Mass budgets for perchloroethylene (PCE), trichloroethylene (TCE), dichloroethylene (DCE), and vinyl chloride (VC) for a case of dense nonaqueous phase liquid remediation under low pumping conditions. NAPL, nonaqueous phase liquid.

The low hydraulic conductivity of the system is responsible for the large cleanup times, even with the aggressive cleanup strategies that were examined. Furthermore, persistence of contaminants in the unsaturated zone is a result of diffusion in air and water being the only mechanisms for transport above the water table.

The fifth simulation study considers air sparging and vacuum extraction. A sparge well is located within the NAPL plume, 6 m downstream of the left edge of the domain, at a height of 0.5 m above the bottom. The vacuum extraction well is located 5 m downstream of the left edge of the domain, at a height of 3.75 m above the bottom. The paved land surface is assumed to be a no-flow boundary condition to air. Water table conditions are the same as shown in Fig. 3; however, advective transport of contaminants in the water phase is neglected in this simulation. Figure 7 shows the mass balance components of PCE, TCE, DCE, and VC with time for this case. Total cleanup is much more rapid than the water-phase remedial technologies, with the domain being clean of NAPL phase within 120 d. However, it should be noted that significant contaminant mass exits the lateral boundaries of the simulation domain, possibly spreading the contaminant; it is therefore important that the vacuum extraction wells be designed properly to entirely capture the flow from the sparge.

This example demonstrates how various system designs may be evaluated to meet the different objectives at a complex contaminated site. For the case under investigation, air sparging with vacuum extraction caused most rapid cleanup, but these systems may be difficult and costly to install and operate and may spread contaminants in the subsurface if not designed properly. A high rate of pumping was the next most effective technology in terms of cleanup times, but the ecological impacts of large drawdowns, the high cost of high pumping, and disposal of treated water are issues that need to be addressed. Lower pumping rates did not protect the compliance point, but injection of the treated water downstream of the extraction point provided sufficient dilution to reduce concentrations reaching the downstream edge below MCLs. The flexible analysis capabilities of MODFLOW SURFACT enable this complex set of analyses to be performed from early pilot studies, site characterization, ambient flow analyses, to investigations of impacts of various cleanup technologies.

Problem 2: Examination of Contaminant Movement in a Fractured System

This example demonstrates the behavior of dual domain systems and shows the significance of appropriate representations for such settings. A site exhibited cleanup to very low levels with significant rebound of concentrations when the pumps were turned off. Further geologic and hydrogeologic investigations confirmed a characteristic dual porosity behavior. Preliminary modeling was conducted for a quick analysis to investigate this behavior and assess significant mechanisms for remedial design considerations. A 88.4- by 88.4-m rectangular domain was constructed over the contaminated area, over the 3-m thickness of the plume. Due to low ambient gradients, they were neglected to further focus the investigation on significance of the dual domain mechanisms. Water was extracted from the center of the study area under various design settings, with a uniform and constant head value along

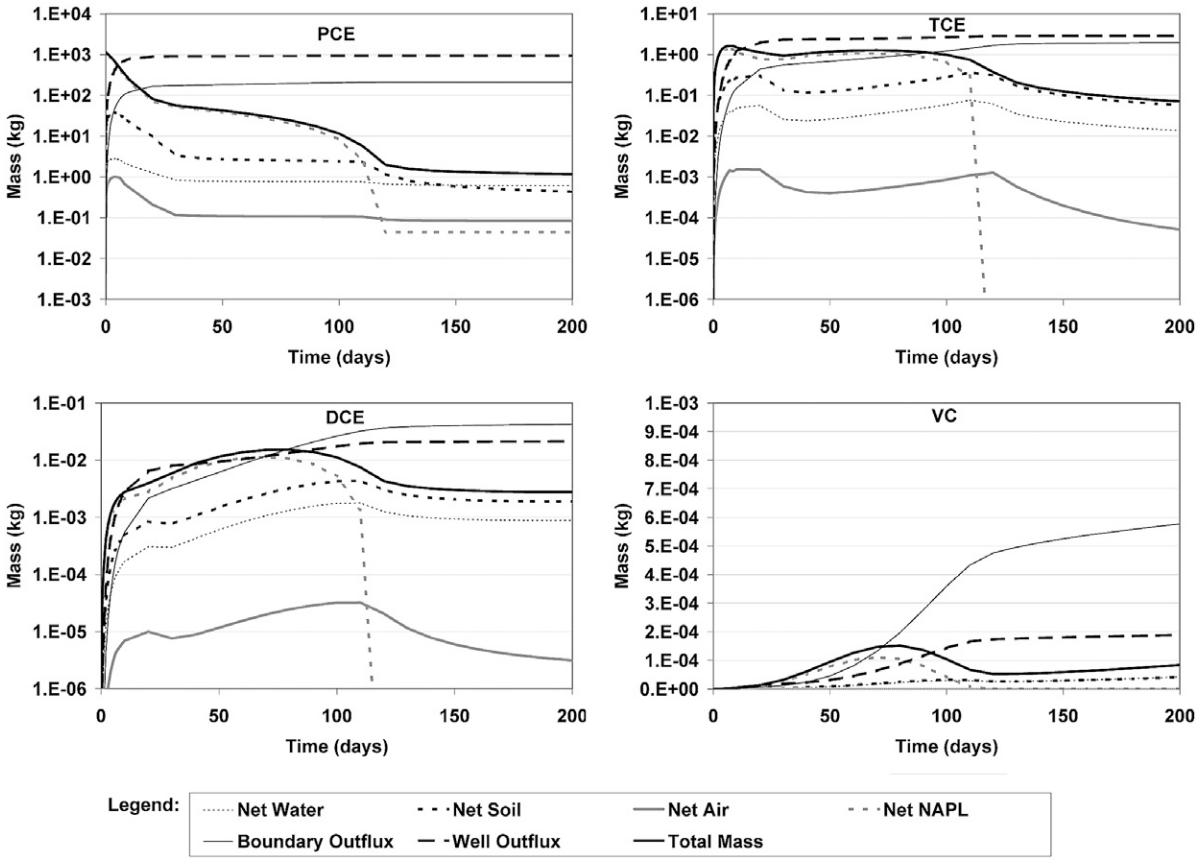

FIG. 7. Mass budgets for perchloroethylene (PCE), trichloroethylene (TCE), dichloroethylene (DCE), and vinyl chloride (VC) for a case of dense nonaqueous phase liquid remediation under air sparging conditions. NAPL, nonaqueous phase liquid.

lateral boundaries allowing freshwater into the domain as a result of pumping. Table 5 shows the parameter values used for the contaminant and the site under study.

The simulations were initiated with a relative concentration of contaminant equal to unity in both the mobile and immobile domains throughout the study area. Simulations were performed for 8000 d (almost 22 yr) to investigate the mass extracted by the well and concentrations at the extraction well. Figure 8 shows the breakthrough of contaminant at the pumping well for 8000 d, for the various cases studied. Figure 8a shows the cumulative mass extracted, Fig. 8b depicts the simulated concentration in water in the mobile domain (within the fracture system) at the extraction well location, Fig. 8c shows the mass withdrawal rate, and Fig. 8d depicts the simulated concentration in water in the immobile domain (within the matrix block) at the extraction well grid block.

The first simulation considers a pumping rate of 25.5 $m^3\ d^{-1}$ (high pumping case). Relative concentrations in the mobile domain are noted to rapidly drop to below 0.06 within 170 d but stay high in the immobile domain. Mass removal rates are also high initially but drop off rapidly, as mass transfer between immobile and mobile domains becomes the controlling factor. Mass removed by the well is approximately 2.2×10^5 units by 8000 d. The second simulation considers a pumping rate of 2.6 $m^3\ d^{-1}$ (low pumping case). The concentration breakthrough in the mobile domain is much slower here than for the higher pumping case, dropping to about 0.1 in 8000 d. Cumulative mass extracted by the well is, however, only slightly lower than for the first simulation, which initially extracts higher amounts of contaminant from the fracture domain, with contaminant extraction rates being similar at later times. This depicts the classic dual porosity behavior where the mass transfer rate between domains controls the mass removal from the system. The third simulation considers a pulsed pumping of 25.5 for 200 d, followed by no pumping for 200 d—with this sequence continuing for 8000 d. This operational design suggests itself from the previous simulations, which show

TABLE 5. Simulation properties for dual porosity example.

Property	Value
Hydraulic conductivity of the system	0.305 m d^{-1}
Mobile fraction	1×10^{-1}
Longitudinal dispersivity	8.96×10^{-2} m
Transverse dispersivity	0 m
Porosity	
In mobile domain	
In immobile domain	0.25
Retardation Coefficient R	
In mobile domain	1.0
In immobile domain	2.0
Decay coefficient λ	
In mobile domain	0 d^{-1}
In immobile domain	0 d^{-1}
Diffusion coefficient	0 $m^2\ d^{-1}$
Mass transfer rate between domains	1.0×10^{-4} d^{-1}

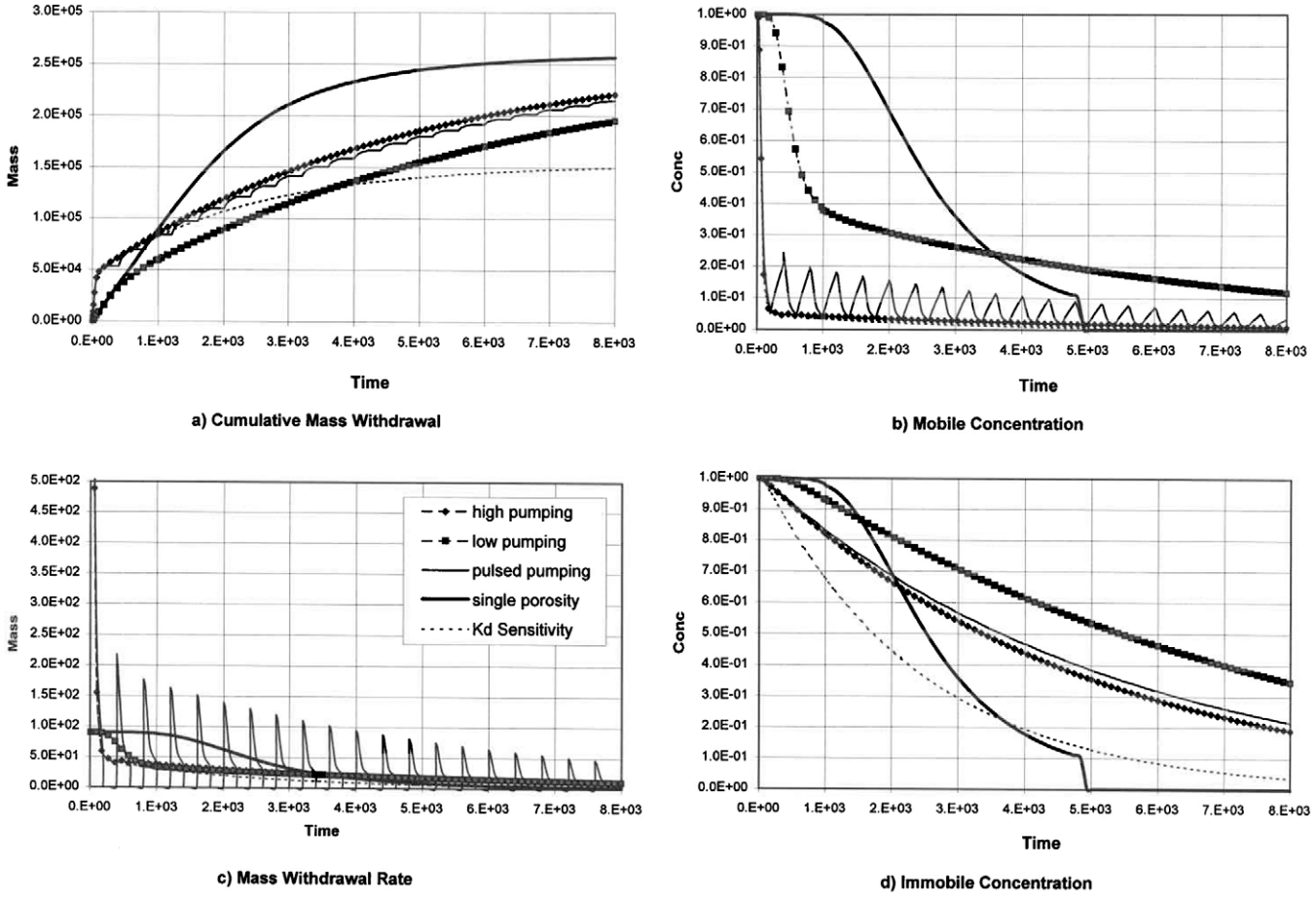

FIG. 8. Contaminant breakthrough within a dual domain system for various pumping conditions. K_d, soil–water partitioning coefficient.

a loss of effectiveness of high or low pumping rates after 200 d. Relative concentration in the mobile domain drops rapidly to 0.06 in 170 d (as it did for the first simulation) but rises back to about 0.2 during the recovery period, as contaminants move out of the immobile domain. This behavior is noted in the field with even more rapid concentration breakthroughs for higher pumping rates. Mass removed by this design was approximately 2.1×10^5 units by 8000 d, which is very similar to mass removal by continuous operation at the higher pumping rate and is in fact not much higher than continuous operation at an order of magnitude lower pumping rate of the second simulation. The pulsed case also shows a decrease in effectiveness with time and lower pumping rates with larger rebound intervals at later times would prove even more efficient.

Assumptions for this investigation include the following: rock and fracture storage effects are neglected (steady-state flow); advection between media is neglected (during startup, or for the pulsed scenario, advection between media might be a consideration in regions near the well where pressures changes can be large); and contaminant, being present over several decades within the subsurface, has equilibrated into the immobile domain, with initial relative concentrations of unity equal to that within the mobile domain.

Equivalent porous medium (single porosity) simulations for the site require unrealistic parameters to even partially fit the observed contaminant behavior. For a pumping rate of 25.5 m^3 d^{-1}, the single porosity model takes 10 yr to drop concentrations down to about 0.1 using representative porosity values obtained from the field, while these concentrations drop rapidly for the dual domain simulations. The single porosity simulation further shows a more effective system than is possible in the field, having higher mass removal rates for much longer periods than the dual domain simulations.

An interesting sensitivity simulation worth noting here is the sensitivity to retardation in the immobile domain. An unretarded simulation (retardation coefficient = 1 in the matrix domain) showed similar concentration breakthrough in the mobile domain and similar early mass withdrawal rates for a high pumping (25.5 m^3 d^{-1}) simulation; however, cumulative mass extraction was much lower, at 1.5×10^5 units by 8000 d, and immobile domain concentrations breakthroughs were quite different. Retardation affects calculations of in-place initial mass, with more mass residing on the soil when retardation is larger. The initial mass is often a significant unknown for most situations; therefore, within the range of retardation coefficients for a system, long-term mass extraction projections can be significantly different. Thus, examining early mass withdrawal rates and mobile phase concentrations do not provide a significant indicator of in-place mass, as does examining the immobile domain's concentration breakthrough, to provide more accurate long-term predictions.

Conclusions

A set of modules has been developed and incorporated into the USGS groundwater flow simulation code, MODFLOW, to enhance its simulation capabilities by including a wide variety of commonly occurring situations encountered in the field. These modules utilize the basic unsaturated zone flow and transport equations in various forms to provide expanded simulation capabilities without solving for multiple coupled equations per node as in multiphase or compositional simulations. Capabilities include a stable unconfined flow formulation; an unsaturated zone water flow formulation in porous or fractured settings; inclusion of well hydraulics and wellbore flow; air flow simulation capabilities for porous or fractured settings above and below the water table for examining air sparging (injection below the water table) and vacuum extraction strategies; multicomponent transport simulations in porous or fractured settings; multiphase transport from an immobile NAPL source; and reactive transport in porous or fractured settings. Accurate mass-conserved numerical schemes are discussed for robust and efficient solution to the set of governing equations.

Two example problems demonstrate application of MODFLOW SURFACT for environmental analyses, the first examining alternatives for a DNAPL remedial design system and the second discussing contaminant movement in a fractured system. These examples depict the complex nature of investigations that can be undertaken by the use of the additional modules. Combinations of these cases can also be simulated because of the modular nature of the simulator. Hence, a field investigation may proceed from preliminary studies to detailed remedial alternative analysis using the same simulation code.

References

Bear, J. 1979. Hydraulics of groundwater. McGraw-Hill, New York.

Behie, G.A., and P.K.W. Vinsome. 1982. Block iterative methods for fully implicit reservoir simulation. Soc. Petrol. Eng. J. 25:658–668.

Blunt, M., and B. Rubin. 1992. Implicit flux limiting schemes for petroleum reservoir simulation. J. Comput. Phys. 102:194–210.

Brooks, R.H., and A.T. Corey. 1966. Properties of porous media affecting fluid flow. J. Irrig. Drain. Div. Am. Soc. Civ. Eng. 92:61–88.

Brusseau, M.L., Z. Gerstl, D. Augustijn, and P.S.C. Rao. 1994. Simulating solute transport in an aggregated soil with the dual-porosity model: Measured and optimized parameter values. J. Hydrol. 163:187–193.

Burnett, R.D., and E.O. Frind. 1987. Simulation of contaminant transport in three dimensions: 2. Dimensionality effects. Water Resour. Res. 23:695–705.

Celia, M.A., E.T. Bouloutas, and R.L. Zarba. 1990. A general mass-conservative numerical solution for the unsaturated flow equation. Water Resour. Res. 27:1483–1496.

Cheng, X., and M.P. Anderson. 1993. Numerical simulation of ground-water interaction with lakes allowing for fluctuating levels. Ground Water 31:929–933.

Clement, T.P. 1997. RT3D: A modular computer code for simulating reactive multi-species transport in 3-dimensional groundwater aquifers. Available online at http://bioprocess.pnl.gov/publictn/PNNL_11720_RT3Dv1_Manual.pdf (verified 6 Mar. 2008). PNNL-11720. Pacific Northwest National Lab., Richland, WA.

Coats, K.H., and B.H. Smith. 1964. Dead-end pore volume and dispersion in porous media. Soc. Petrol. Eng. J. 4:73–93.

Cooley, R.L. 1983. Some new procedures for numerical solution of variably saturated flow problems. Water Resour. Res. 19:1271–1285.

Corapcioglu, M.Y., and S. Panday. 1991. Compositional multiphase flow models. p. 1–59. *In* M.Y. Corapcioglu (ed.) Advances in porous media. Vol 1. Elsevier, Amsterdam.

Fenske, J.P., S.A. Leake, and D.E. Prudic. 1996. Documentation of a computer program (RES1) to simulate leakage from reservoirs using the modular finite-difference ground-water flow model (MODFLOW). Open-File Report 96-364. USGS, Reston, VA.

Finsterle, S., C. Doughty, M.B. Kowalsky, G.J. Moridis, L. Pan, T. Xu, Y. Zhang, and K. Pruess. 2008. Advanced vadose zone simulations using TOUGH. Vadose Zone J. 7:601–609 (this issue).

Forsyth, P.A. 1994. Three-dimensional modeling of steam flush for DNAPL site remediation. Int. J. Numer. Methods Fluids 19:1055–1081.

Gelhar, L.W., and M.A. Collins. 1971. General analysis of longitudinal disper-

sion in nonuniform flow. Water Resour. Res. 7:1511–1521.
Goode, D.J., and C.A. Appel. 1992. Finite-difference interblock transmissivity for unconfined aquifers and for aquifers having smoothly varying transmissivity. Water-Resources Investigations Report 92-4124. USGS, Reston, VA.
Gwo, J.P., P.M. Jardine, G.V. Wilson, and G.T. Yeh. 1995. A multiple-pore-region concept to modeling mass transfer in subsurface media. J. Hydrol. 164:217–234.
Harbaugh, A.W., and M.G. McDonald. 1996a. Programmer's documentation for MODFLOW-96, an update to the U.S. Geological Survey modular finite-difference ground-water flow model. Open-File Report 96-486. USGS, Reston, VA.
Harbaugh, A.W., and M.G. McDonald. 1996b. User's documentation for MODFLOW-96, an update to the U.S. Geological Survey modular finite-difference ground-water flow model: U.S. Geological Survey Open-File Report 96-485. USGS, Reston, VA.
Harten, A. 1983. High resolution schemes for hyperbolic conservation laws. J. Comput. Phys. 49:357–393.
Hill, M.C. 1994. Preconditioned Conjugate-Gradient 2 (PCG2), a computer program for solving groundwater flow equations. Water Resources Investigations Report 90-4048. USGS, Reston, VA.
Hoopes, J.A., and D.R. Harleman. 1967. Wastewater recharge and dispersion in porous media. J. Hydraulics Div. Am. Soc. Civ. Eng. 93:51–71.
Hsieh, P.A., and J.R. Freckleton. 1993. Documentation of a computer program to simulate horizontal-flow barriers using the U.S. Geological Survey's modular three-dimensional finite-difference ground-water flow model. Open-File Report 92-477. USGS, Reston, VA.
Huang, K., B.P. Mohanty, F.J. Leij, and M.Th. van Genuchten. 1998. Solution of the nonlinear transport equation using modified Picard iteration. Adv. Water Resour. 21:237–249.
Huang, K., B.P. Mohanty, and M.Th. van Genuchten. 1996. A new convergence criterion for the modified Picard iteration method to solve the variably-saturated flow equation. J. Hydrol. 178:69–91.
Huyakorn, P.S., B.H. Lester, and J.W. Mercer. 1983. An efficient finite element technique for modeling transport in fractured porous media: 1. Single species transport. Water Resour. Res. 19:841–854.
Huyakorn, P.S., J.W. Mercer, and D.S. Ward. 1985. Finite element matrix and mass balance computational schemes for transport in variably saturated porous media. Water Resour. Res. 21:346–358.
Huyakorn, P.S., S. Panday, and Y.S. Wu. 1994a. A three-dimensional multiphase flow model for assessing NAPL contamination in porous and fractured media: 1. Formulation. J. Contam. Hydrol. 16:109–130.
Huyakorn, P.S., and G.F. Pinder. 1983. Computational methods in subsurface flow. Academic Press, London.
Huyakorn, P.S., E.P. Springer, V. Guvanasen, and T.D. Wadsorth. 1986. A three-dimensional finite element model for simulating water flow in variably saturated porous media. Water Resour. Res. 22:1790–1808.
Huyakorn, P.S., Y.S. Wu, and N.S. Park. 1994b. An improved sharp-interface model for assessing NAPL contamination and remediation in groundwater systems. J. Contam. Hydrol. 16:203–234.
HydroGeoLogic. 1998. MODFLOW-SURFACT v. 3.0: A comprehensive MODFLOW-based flow and transport simulator. Code Documentation Report. HydroGeoLogic, Reston, VA.
Jobson, H.E. 1989. Users manual for an open-channel streamflow model based on the diffusion analogy. Water-Resources Investigations Report 89-4133. USGS, Reston, VA.
Jones, W.F., and B.P. Gibbs. 1995. Flow and transport model of the SRS OBG, using data fusion modeling. Technical report submitted to the U.S. Dep. of Energy, Office of Technology Development. CMB95/328.
Kaluarachchi, J.J., and J.C. Parker. 1989. An efficient finite element method for modeling multiphase flow. Water Resour. Res. 25:43–54.
Kool, J.B., and M.Th. van Genuchten. 1991. HYDRUS: One-dimensional variably saturated flow and transport model, including hysteresis and root water uptake, v.3.31. U.S. Salinity Laboratory, USDA, ARS, Riverside, CA.
Larsbo, M., S. Roulier, F. Stenemo, R. Kasteel, and N. Jarvis. 2005. An improved dual-permeability model of water flow and solute transport in the vadose zone. Vadose Zone J. 4:398–406.
Leake, S.A., and M.R. Lilly. 1997. Documentation of a computer program (FHB1) for assignment of transient specified-flow and specified-head boundaries in applications of the modular finite-difference ground-water flow model (MODFLOW). Open-File Report 97-571. USGS, Reston, VA.
Leake, S.A., and D.E. Prudic. 1991. Documentation of a computer program to simulate aquifer-system compaction using the modular finite-difference ground-water flow model. Book 6, Chapter A2, Open-File Report 88-482. USGS, Reston, VA.
Lester, D.H., G. Jansen, and H.C. Burkholder. 1975. Migration of radionuclide chains through an adsorbing medium. AICHE Symp. Ser. 71(152):202–213.
McDonald, M.G., and A.W. Harbaugh. 1988. A modular three-dimensional finite-difference groundwater flow model. Techniques of Water-Resources Investigations Book 6, Chapter A1. USGS, Reston, VA.
McDonald, M.G., A.W. Harbaugh, B.R. Orr, and D.J. Ackerman. 1991. A method of converting no-flow cells to variable-head cells for the U.S. Geological Survey modular finite-difference ground-water flow model. Open-File Report 91-536. USGS, Reston, VA.
Mohanty, B.P., R.S. Bowman, J.M.H. Hendrickx, and M.Th. van Genuchten. 1997. New piecewise-continuous hydraulic functions for modeling preferential flow in an intermittent-flood-irrigated field. Water Resour. Res. 22:2049–2063.
Mualem, Y. 1976. A new model for predicting the hydraulic conductivity of unsaturated porous media. Water Resour. Res. 12:513–522.
Neuman, S.P. 1972. Theory of flow in unconfined aquifers considering delayed response of the water table. Water Resour. Res. 8:1031–1045.
Ogata, A., and R.B. Banks. 1961. A solution of the differential equation of longitudinal dispersion in porous media. Professional Paper No. 411-A. USGS, Washington, DC.
Panday, S., and M.Y. Corapcioglu. 1989. Reservoir transport equations by compositional approach. Transp. Porous Media 4:369–393.
Panday, S., P.A. Forsyth, R.W. Falta, Y.S. Wu, and P.S. Huyakorn. 1995. Considerations for robust compositional simulations of subsurface nonaqueous phase liquid contamination and remediation. Water Resour. Res. 31:1273–1289.
Panday, S., P.S. Huyakorn, R. Therrien, and R.L. Nichols. 1993. Improved three-dimensional finite-element techniques for field simulation of variably saturated flow and transport. J. Contam. Hydrol. 12:3–33.
Panday, S., Y.S. Wu, P.S. Huyakorn, and E.P. Springer. 1994. A three-dimensional multiphase flow model for assessing NAPL contamination in porous and fractured media: 2. Porous medium simulation examples. J. Contam. Hydrol. 16:131–156.
Papadopoulos, I.S., and H.H. Cooper, Jr. 1967. Drawdown in a well of large diameter. Water Resour. Res. 3:241–244.
Porter, D.W., B.P. Gibbs, W.F. Jones, P.S. Huyakorn, L.L. Hamm, and G.P. Flach. 2000. Data fusion modeling for groundwater systems. J. Contam. Hydrol. 42:303–335.
Prudic, D.E. 1989. Documentation of a computer program to simulate stream-aquifer relations using a modular finite-difference ground-water flow model. Open-File Report 88-729. USGS, Reston, VA.
Pruess, K. 2004. The TOUGH codes: A family of simulation tools for multiphase flow and transport processes in permeable media. Vadose Zone J. 3:738–746.
Pruess, K., and T.N. Narasimhan. 1985. A practical method for modeling fluid and heat flow in fractured porous media. Soc. Petrol. Eng. J. 25:14–26.
Scheidegger, A.E. 1961. General theory of dispersion in porous media. J. Geophys. Res. 66:3273–3278.
Shan, C. 1995. Analytical solutions for determining vertical air permeability in unsaturated soils. Water Resour. Res. 31:2193–2200.
Šimůnek, J., N.J. Jarvis, M.Th. van Genuchten, and A. Gardenas. 2003. Review and comparison of models for describing non-equilibrium and preferential flow and transport in the vadose zone. J. Hydrol. 272:14–35.
Šimůnek, J., D.L. Suarez, and M. Sejna. 1996. The UNSATCHEM software package for simulating the one-dimensional variably saturated water flow, heat transport, carbon dioxide production and transport, and multicomponent solute transport with major ion equilibrium and kinetic chemistry. Version 2.0. Research Report No. 141. U.S. Salinity Laboratory, USDA-ARS, Riverside, CA.
Sudicky, E.A., A.J.A. Unger, and S. Lacombe. 1995. A noniterative technique for the direct implementation of well bore boundary conditions in three-dimensional heterogeneous formations. Water Resour. Res. 31:411–415.
Swain, E.D., and E.J. Wexler. 1993. A coupled surface-water ground-water model for simulation of stream-aquifer interaction. Open-File Report 92-138. USGS, Reston, VA.
Theis, C.V. 1935. The relation between the lowering of the piezometric surface and the rate and duration of discharge of a well using groundwater storage.

Trans. Am. Geophys. Union 16:519–524.
Unger, A.J.A., P.A. Forsyth, and E.A. Sudicky. 1996. Variable spatial and temporal weighting schemes for use in multiphase compositional problems. Adv. Water Resour. 19:1–27.
van Genuchten, M.Th. 1980. A closed-form equation for predicting the hydraulic conductivity of unsaturated soils. Soil Sci. Soc. Am. J. 44:892–898.
van Genuchten, M.Th. 1981. Non-equilibrium transport parameters from miscible displacement experiments. Res. Rep. 119. U.S. Salinity Laboratory, Riverside, CA.
van Genuchten, M.Th., and F.N. Dalton. 1986. Models for simulating salt movement in aggregated field soils. Geoderma 38:165–183.
van Genuchten, M.Th., G.F. Pinder, and W.P. Saukin. 1977. Modeling of leachate and soil interactions in an aquifer. p. 95–103. *In* Management of gas and leachate in landfills. Rep. EPA-600/9-77-026. USEPA, Cincinnati, OH.
van Genuchten, M.Th., and P.J. Wierenga. 1976. Mass transfer studies in sorbing porous media: I. Analytical solutions. Soil Sci. Soc. Am. J. 40:473–480.
van Leer, B. 1977. Towards the ultimate conservative difference scheme: IV. A new approach to numerical convection. J. Comput. Phys. 23:276–299.
van Leer, B. 1979. Towards the ultimate conservative difference scheme: V. A second-order sequel to Godunov's method. J. Comput. Phys. 32:101–136.
Vogel, T., H.H. Gerke, R. Zhang, and M.Th. van Genuchten. 2000. Modeling flow and transport in a two-dimensional dual-permeability system with spatially variable hydraulic properties. J. Hydrol. 238:78–89.
Wilson, J.L., and P.J. Miller. 1978. Two-dimensional plume in uniform groundwater flow. J. Hydraul. Div. Am. Soc. Civ. Eng. 104:503–514.
Wu, Y.S., P.S. Huyakorn, and N.S. Park. 1994. A vertical equilibrium model for assessing nonaqueous phase liquid contamination and remediation of groundwater systems. Water Resour. Res. 30:903–912.
Wu, Y.S., H.H. Liu, and G.S. Bodvarsson. 2004. A triple-continuum approach for modeling flow and transport processes in fractured rock. J. Contam. Hydrol. 73:145–179.
Zheng, C. 1990. A modular three-dimensional transport model for simulation of advection, dispersion, and chemical reactions of contaminants in groundwater systems. Kerr Environmental Research Laboratory, Ada, OK.